

Soil mechanics and the observational method: challenges at the Zelazny Most copper tailings disposal facility

M. JAMIOLKOWSKI*

This paper illustrates the geotechnical aspects of the development of one of the world's largest copper tailings disposal facilities, located at Zelazny Most in south-west Poland. Its operation commenced in 1977 and, by the end of 2013, $527 \times 10^6 \text{ m}^3$ of tailings had already been stored within a confining embankment dam ('ring dam') of about 14.3 km in total length. The foundations of the ring dam lie on Pleistocene deposits, underlain by a thick sequence of Pliocene sediments. The period of operation of the facility will continue until exhaustion of the ore body, which is estimated to occur in 2042, when the total volume of tailings stored will reach $1000 \times 10^6 \text{ m}^3$. The development and the use of the Zelazny Most facility is affected by a number of significant geotechnical hazards, including the phenomenon of flow liquefaction, as is often the case for such structures. However, the most important geotechnical hazard at Zelazny Most is a consequence of its location in an area that, during the Pleistocene, experienced at least three major glaciations. The ice sheets, over 1000 m thick, which overrode the area, induced substantial glacio-tectonic phenomena, the most geotechnically important of which is the formation of extensive sub-planar shear planes in the Pliocene clays that extend to depths of around 100 m. The shear strength in these shear zones, which occur mostly in high-plasticity clays, is close to residual, thus controlling the stability of the confining dams. Moreover, the area of the disposal is also subject to a moderate degree of mining-induced seismicity. Discussion of this is omitted from this paper because of its relatively minor influence on the design of the depository. Given the large scale of the disposal facility, the complexity of the geological and geotechnical settings, and its anticipated life span, the owners KGHM (the Polish acronym for Copper Mine and Mill Company), on the advice of the World Bank, appointed an international board of experts (IBE). The IBE, supported by a Polish geotechnical expert as local liaison, have the responsibility to oversee the safe development of the tailings dams by applying Peck's observational method. This paper describes the monitored behaviour of the dams, with particular reference to the presence of the glacio-tectonic phenomena and the remedial measures adopted for their mitigation. The geotechnical characterisation of the foundation soils and of the tailings is described, and the stability analyses of the tailings dams are discussed in the context of the safe development of the whole facility.

KEYWORDS: clays; dams; glacial soils; liquefaction; mining; remediation

INTRODUCTION

This paper describes the geotechnical aspects of the development of one of the world's largest copper tailings disposal facilities, located at Zelazny Most in south-west Poland, close to the borders with the Czech Republic and Germany (see Fig. 1). KGHM (the Polish acronym for Copper Mine and Mill Company), the government-owned mining company, started mining the copper ore body in 1972, and plans to continue until exhaustion of the ore, which is estimated to occur in 2042. By the end of 2013, $527 \times 10^6 \text{ m}^3$ of tailings had been stored in the disposal facility, consistent with an average storage rate of $17 \times 10^6 \text{ m}^3/\text{year}$, with a maximum dam height approaching 63 m. An aerial view of the Zelazny Most disposal facility is shown in Fig. 2, together with further data on the confining ring dam.

As with all tailing dams, the Zelazny Most disposal poses a number of challenges for the geotechnical engineer, in particular flow liquefaction of the stored tailings, which potentially threatens the stability of the confining dams. This in turn depends on the height of the dam and on the mechanical behaviour of the foundation soils. This latter



Fig. 1. Location of the Zelazny Most depository

issue, as will be seen, has turned out to be the main factor controlling the development of the disposal, a consequence of the complex Pleistocene geological history of the area.

KGHM, in 1992, appointed a four-member international board of experts (IBE): Dr David Carrier (USA); Professor Richard Chandler (UK); Professor Kaare Høeg (Norway); and Professor Michele Jamiolkowski (Italy). The IBE was

Manuscript received 23 June 2014; revised manuscript accepted 1 July 2014.

Discussion on this paper closes on 1 January 2015, for further details see p. ii.

* Technical University of Torino, Italy.



Maximum dam height: 63 m
 Total volume stored: $527 \times 10^6 \text{ m}^3$
 Storage rate: $\approx 17.5 \times 10^6 \text{ m}^3/\text{year}$
 Area covered: 12.4 km^2
 Total length of dam: 14.3 km

Fig. 2. Aerial view of the Zelazny Most depository

assigned the task, in cooperation with the Polish geotechnical expert, Professor Wojciech Wolski, of overseeing the safe development of the tailings dams by applying the observational method (Peck, 1969, 1980; Jamiolkowski *et al.*, 2010).

Within the framework of this on-going project, for which the overall period of operation will exceed 70 years, the application of the observational method as conceived by the IBE consists of the following stages

- (a) continuous enhancement of the monitoring network, and of the communication system between the monitoring groups and the end users of the results of monitoring
- (b) geotechnical analyses of the observed displacements of the dams so as to predict their further evolution with the continuing increase of dam height with time
- (c) modification of the plans for design and construction in the light of the monitoring results and stability analyses.

TAILINGS DISPOSAL

The Zelazny Most dam, which completely surrounds the tailings disposal, will hereafter be referred as the ‘ring dam’. The original ground surface where the disposal facility is placed was saddle-shaped, so that the eastern and western portions of the ring dam are higher than those to the north and south. The present elevation of the crest of the ring dam ranges between 177 m and 177.5 m above sea level (asl). A plan view to show the dam heights above the original downstream ground level is given in Fig. 3.

The Zelazny Most tailings dam is being raised using the upstream construction method (see Fig. 4). The shell of the dam is built using the coarser tailings, which are fine sand with a low-plasticity ($I_p \leq 10\%$) silt fraction, separated from the remainder of the tailings by spigotting. The construction of the Zelazny Most starter dam from local earthen material began in 1975, and the storage of tailings started in 1977. Since then, the dam crest has risen at a rate of approximately 1.0 to 1.5 m/year, constructed with an average downstream slope of 3.5 horizontal to 1 vertical. Furthermore, the beach (i.e. the distance from the dam crest to the pond edge) is maintained with a length of not less than 200 m. These conservative practices have the effect that the finest tailings, the softer, weaker ‘slimes’, are deposited closer to the pond, and a thick, strong dilative dam shell is formed.

To keep the phreatic surface in the shell depressed, in addition to the toe drain, four levels of circumferential

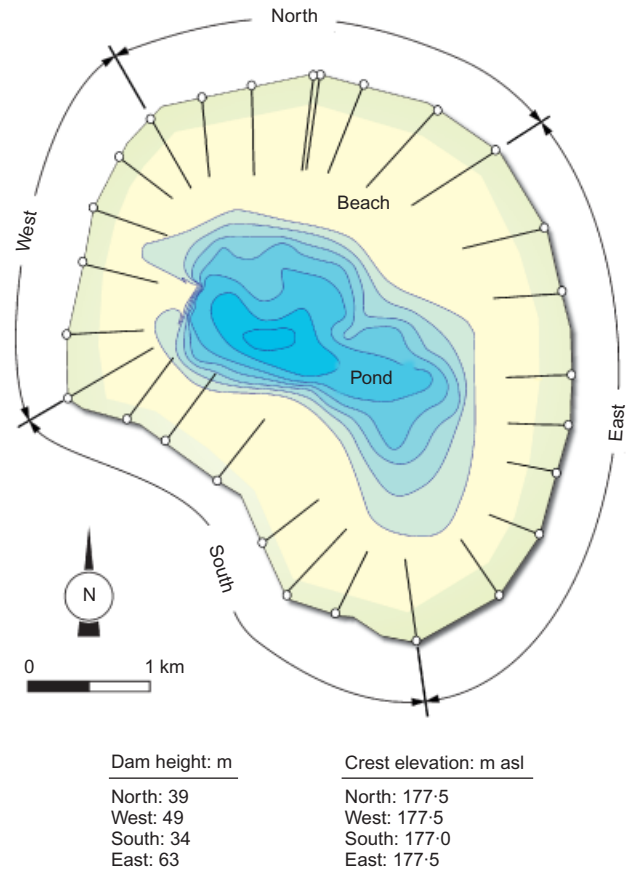


Fig. 3. Dam height and crest elevation (updated December 2013)

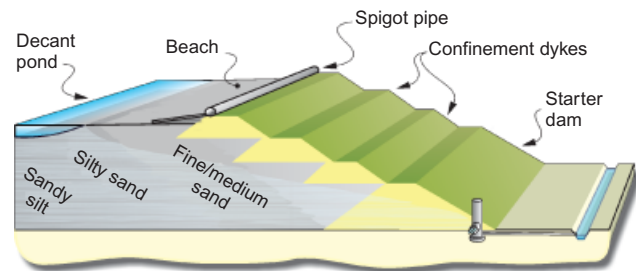


Fig. 4. Ring dam: schematic cross-sections

drains have been installed as the dam was raised (see Fig. 5). Further circumferential drains will be added as the dam is raised further. As will be described in the later section on ‘Behaviour of the ring dam’, this drainage system has proved to be efficient, and has considerably reduced the risk of flow failure of the tailings, so that the dam stability is now effectively controlled by the foundation soils.

The tailings disposal facility at Zelazny Most is roughly half complete. Its further development will be monitored by a rigorous and continuously enhanced application of the observational method, combined with a feasibility study examining different deposition technologies, aimed at reducing the enormous volume ($500 \times 10^6 \text{ m}^3$) still to be stored in the disposal.

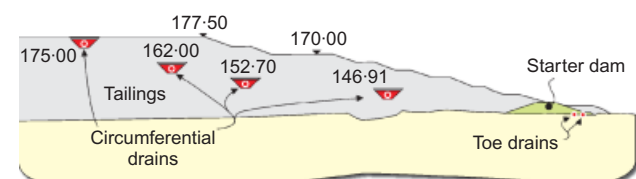


Fig. 5. Ring dam: circumferential drains

LOCAL GEOLOGY

The Zelazny Most tailings depository is located in a complex geological environment. From the ground surface downwards, the foundation soils consist of Pleistocene deposits, including silty lake clays and out-wash sands, rare sandy gravel inclusions and silty sands. These are underlain by thick layers of freshwater, medium- to high-plasticity Pliocene clays, which incorporate thin, brown coal and sand strata. The Pliocene deposits overlie Triassic strata, which include beds of halite, below which the copper ore body is encountered.

The complexity of these deposits is the consequence of the Pleistocene history of the area, when a succession of ice sheets moved from north to south over central Europe. At least six major ice advances are recognised in south Poland, no less than three of which have passed over the Zelazny Most area (see Fig. 6). The various ice sheets, which are believed to have been at least 1000 m thick, have induced widespread glacio-tectonic phenomena (see Fig. 7), probably extending to depths of about 100 m, which in particular have greatly affected the Pliocene deposits.

As a consequence, they are intensely sheared, folded and generally severely disturbed. In places, the initially horizontally bedded freshwater Pliocene sediments have Pleistocene deposits thrust within them (see Fig. 8).

These glacio-tectonic phenomena have left a permanent imprint on the Zelazny Most geotechnical environment, in particular the frequent and extended shearing and folding of the Pliocene deposits. The passage of the ice sheets must have imposed a stress field resembling that of simple shear. This has generated several sub-planar shear surfaces that are



Fig. 6. Pleistocene glaciations: maximum extent in south-west Poland

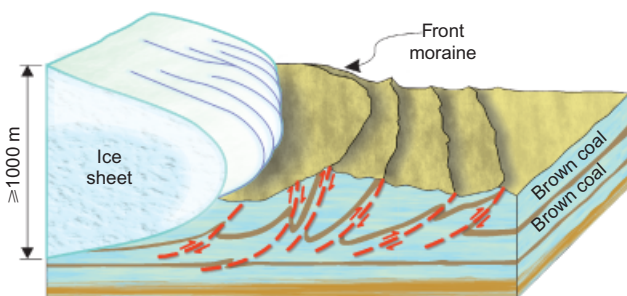


Fig. 7. Deformations ahead of an ice sheet

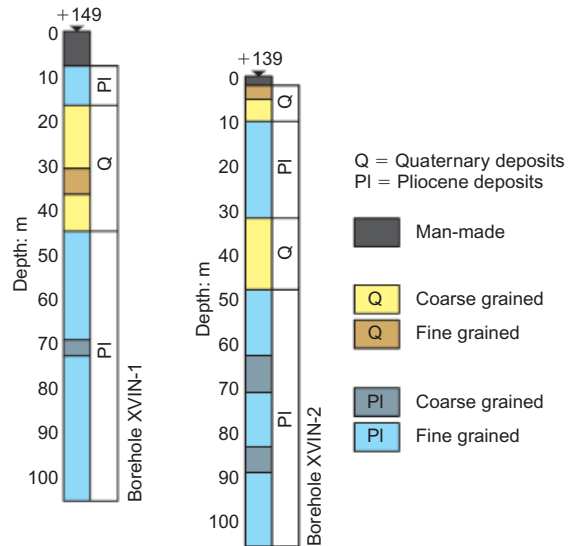


Fig. 8. North dam, section XVIN: borehole log of two nearby borings

highlighted by the inclinometer surveys carried out beyond the toe of the East dam, shown in Fig. 9. Laboratory tests show that these shear surfaces occur particularly in high-plasticity clay and that they have a drained shear strength that is close to the residual. The horizons containing the glacio-tectonic shear planes are probably thin ‘zones’ of high-plasticity slickensided clay. Overall, as a result of the glacio-tectonic disturbance, the Pliocene deposits exhibit an extremely pronounced spatial variability, which makes the formulation of realistic geological and geotechnical models extremely difficult, if not completely impracticable. As an example, Fig. 10 shows an extremely simplified model of

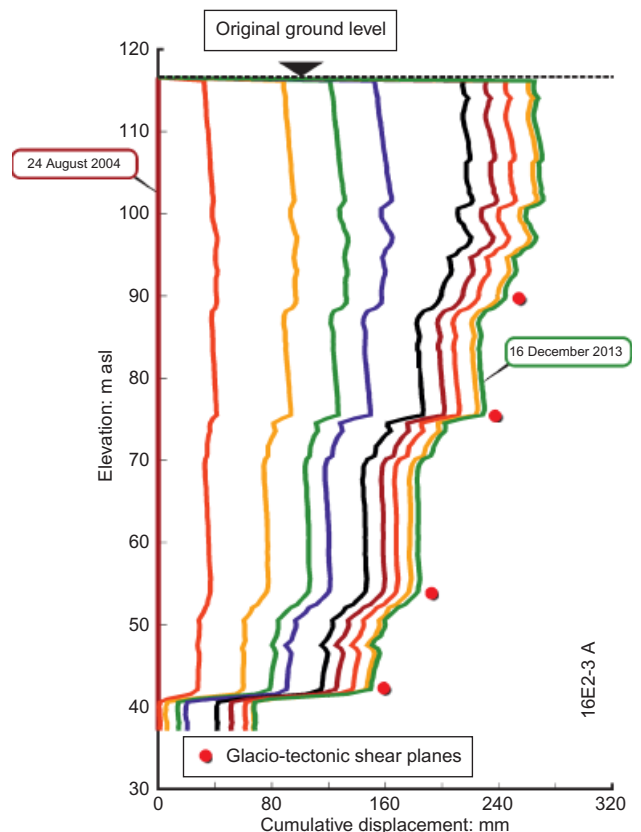


Fig. 9. Inclinometer surveys beyond the East dam toe

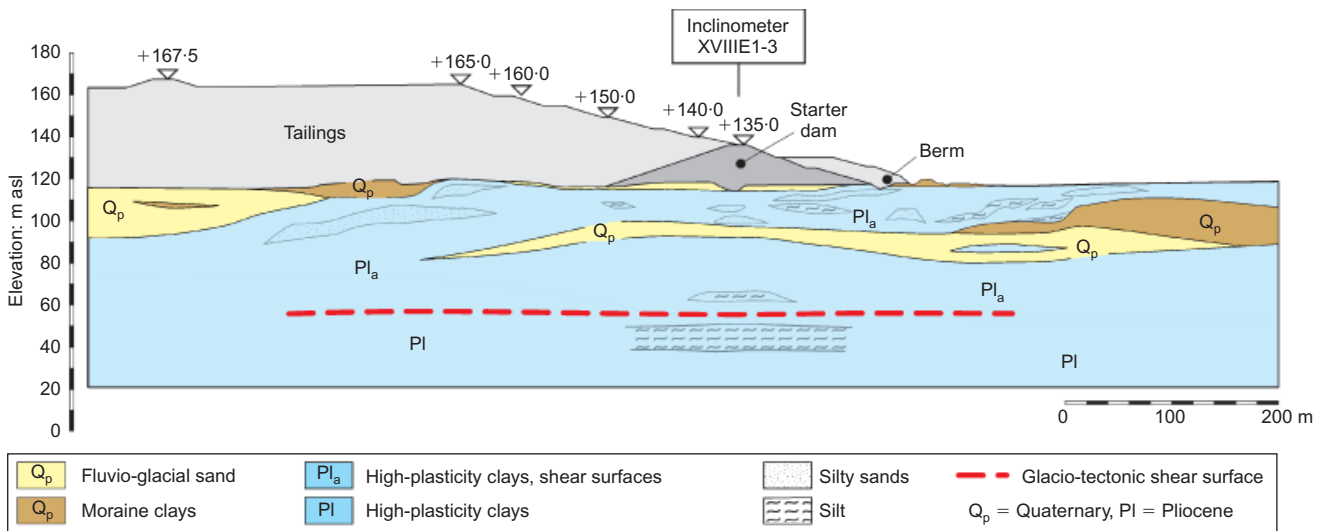


Fig. 10. East dam: simplified soil profile

geotechnical cross-section XVIIE, which neglects many stratigraphy details, and was developed for use in finite-element stress–deformation analysis.

BEHAVIOUR OF THE RING DAM

Having set the scene, this paper now examines how the geology comes to be the major factor controlling the design and the construction of the Zelazny Most tailings facility. This will be done by applying the observational method based on an extensive monitoring system, the most relevant components of which are listed below.

- (a) Over 450 surface bench marks and the heads of more than 55 inclinometers are used; these are surveyed two to four times a year; since 1990 this has included the use of global positioning systems (GPS).
- (b) More than 300 vibrating wire piezometers are used, installed in fully grouted borings, up to 150 m deep (e.g. Vaughan, 1969; Mikkelsen & Green, 2003; DiBiagio & Strout, 2013). Many are installed in boreholes which also contain an inclinometer casing, so that it is possible to compare piezometer records with displacement, particularly in the vicinity of active shear planes.
- (c) Fifty-six inclinometers up to 150 m deep are used. The life of the inclinometers is often limited owing to the large localised shear displacements on the glacio-tectonic shear surfaces. Moreover, in spite of the substantial depth of many of the inclinometer casings, it is now being recognised that the toes of the casings generally are not fixed. Consequently, the interpretation of the inclinometer surveys is carried out ‘top-down’, based on GPS monitoring of the horizontal displacements of the top of the casings.

Figure 11 shows a plan view of the ring dam, which is approximately 14.3 km long, subdivided into spigotting cross-sections (Arabic numerals) and 85 geodetic (Roman numerals) cross-sections.

The four sections shown are on the East and North dams, and all exhibit major glacio-tectonic shear surfaces in the dam foundation.

East dam

The East dam (note that the original elevation of the ground level at the East dam was between 111 and 117 m asl; the elevation of the starter dam was 136 m asl;

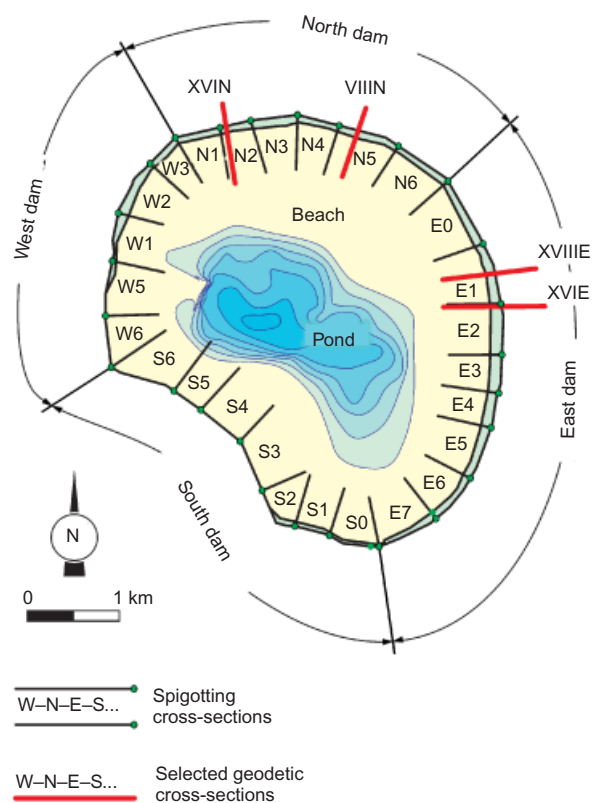


Fig. 11. Tailing disposal plan view, selected geodetic cross-sections

and the depth to ground water level was 1–4 m), the highest portion of the ring dam (presently 63 m high) and which was constructed over an old river bed, was the first portion of the dam to show significant horizontal surface displacements. These have been observed over a distance of 1 km along the dam axis, centred on cross-section XVIIIE. Fig. 12 shows in plan the horizontal displacements of the eastern starter dam, relating to the period 2003–2013. The maximum movements occur near bench marks BM-208 and BM-208.1, located on dam cross-section XVIIIE. Bench mark BM-208 has been monitored since 1981, and by the end of 2013 had shown a total horizontal surface displacement of ≈ 655 mm. The construction history of the East dam, and the horizontal surface displacements of BM-208 since 1981, are shown in Fig. 13. Towards the end of 1995, when the dam crest had

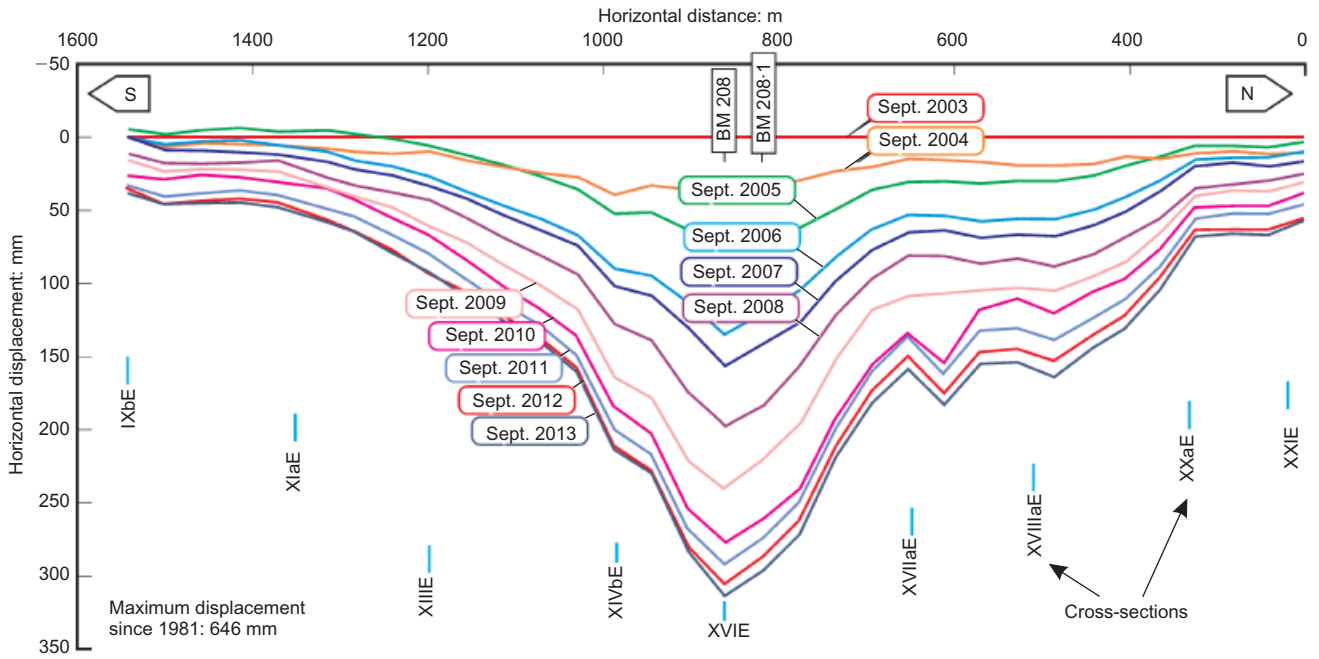


Fig. 12. Eastern starter dam: plan view of horizontal surface displacements

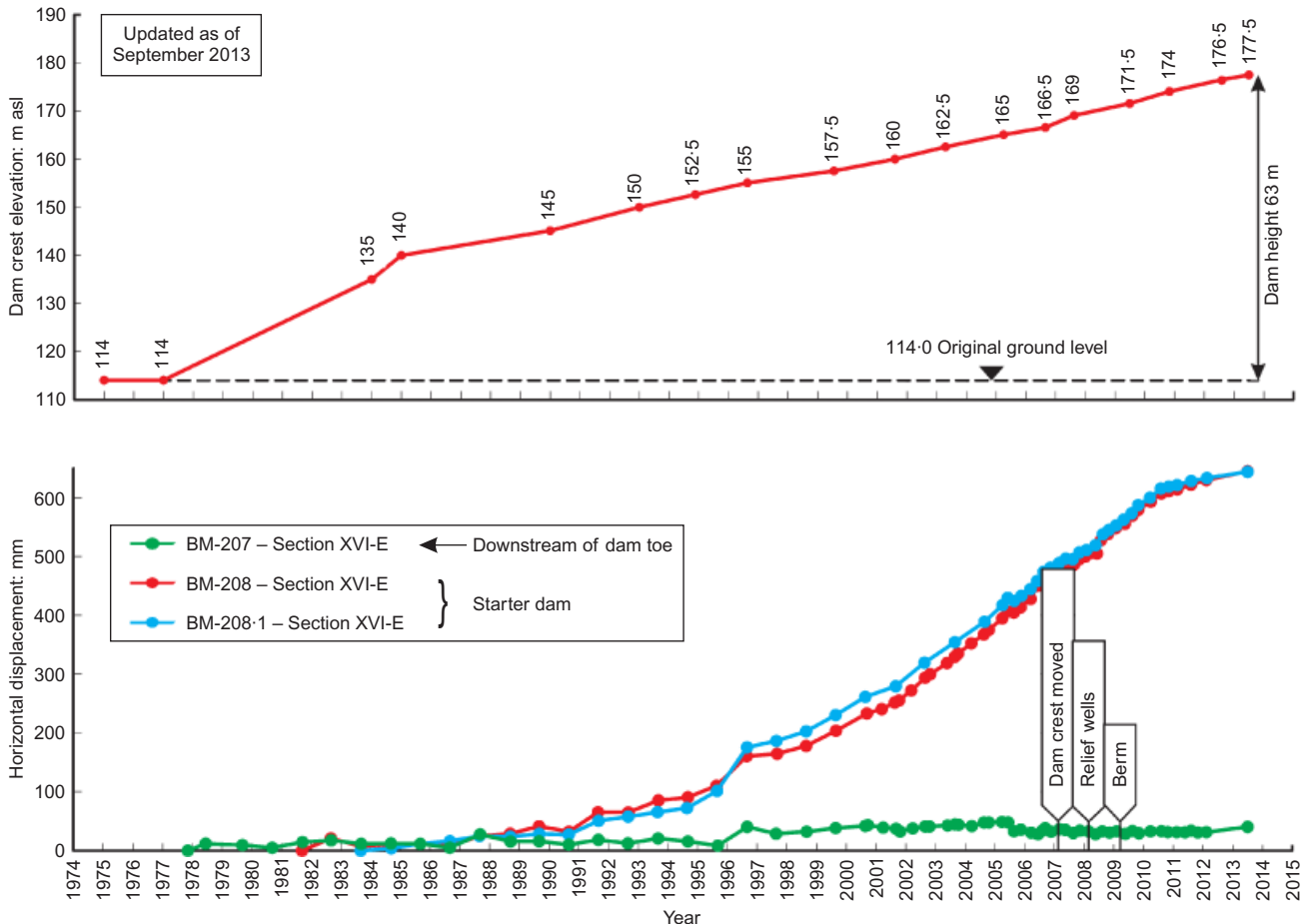


Fig. 13. Cross-section XVIIe: construction history and horizontal surface displacements

reached the height of ≈ 40 m, the rate of horizontal surface displacement increased, so that during 2001–2009 displacement rates were between 40 and 50 mm/year (see Table 1). Fig. 14 shows the general pattern of the horizontal surface displacements and of the settlements of cross-section XVIIe, as well as the numbers of the bench marks.

The deep inclinometers that were installed after 2003 have provided evidence that most movements in the dam foundation are concentrated along sub-horizontal glacio-tectonic shear planes.

Figure 15 shows the surveys of the inclinometers installed in the starter dam, indicating the shear planes re-activated in

Table 1. Horizontal surface displacement rates of BM-208

mm/year	Year
28.3	1999–2000
19.5	2000–2001
41.5	2001–2002
37.1	2002–2003
37.8	2003–2004
38.0	2004–2005
58.9	2005–2006
21.8	2006–2007
41.4	2007–2008*
42.3	2008–2009
48.6	2009–2010
15.3	2010–2011
13.0	2011–2012
9.0	2012–2013

Note: Total displacements from 1981 to December 2013: 646 mm.
 * Start of stabilisation measures.

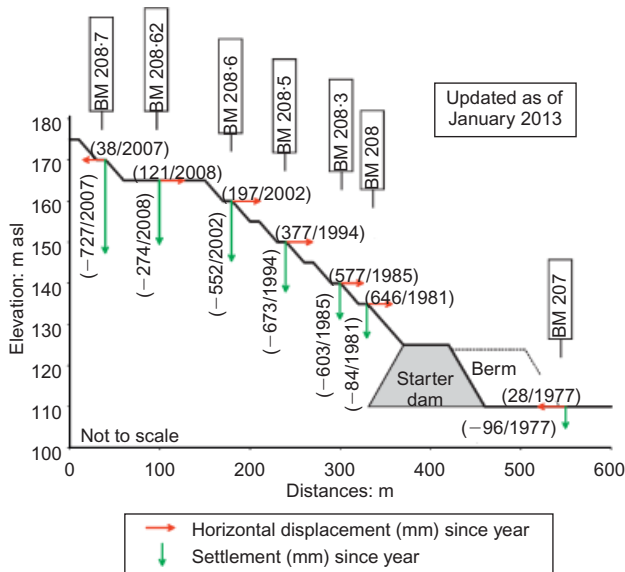


Fig. 14. Cross-section XVIIE: horizontal surface displacements and settlements

cross-sections XVIIE and XVIIIE. In cross-section XVIIE two active shear planes occur, at elevations 75 m and 45 m asl.

Figure 15 shows that in both inclinometer casings the majority of the observed movements occur along the deeper shear surface. This figure presents clear evidence that the toes of the two inclinometers are not fixed. The observed movements beneath the deepest active shear plane can probably be attributed to consolidation and shear deformation of the foundation soils under the load of the dam, although there is just the possibility that there are active shear planes below the inclinometer casing.

The 26 deep inclinometers in this length of the East dam indicate the presence of shear planes at a range of elevations extending both north and south from cross-section XVIIE (Fig. 12), and spread at least 200 to 300 m beneath the width of the dam.

Together, the geodetic and the inclinometer data surveys show that the starter dam and the foundation soil above 45 m asl move virtually as a single, rigid body. This behaviour changes, however, at higher elevations within the dam, where there is a more complex mechanism of movement with depth, as shown in Fig. 16. The inclinometers also exhibit a number of glacio-tectonic shear surfaces at higher

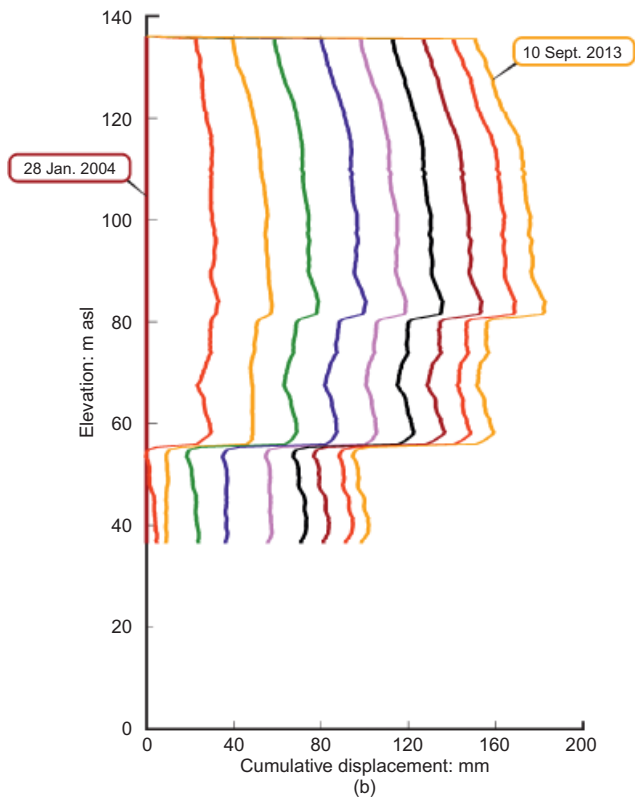
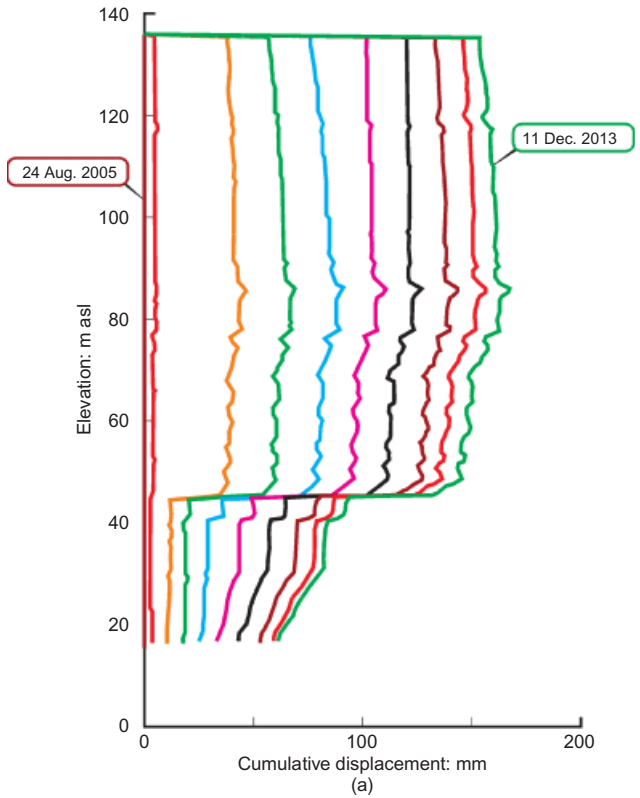


Fig. 15. Eastern starter dam, response of deep inclinometers: (a) 17E-5 A; (b) 18E1-3 A

elevations than that on which main shearing movement is observed. In addition, the maximum horizontal displacement at depth is appreciably larger than that shown by bench marks located on the upper parts of the dam, indicating a rotational component of displacement.

Given the large horizontal displacements and the corresponding displacement rates (see Table 1) during 1999–2010

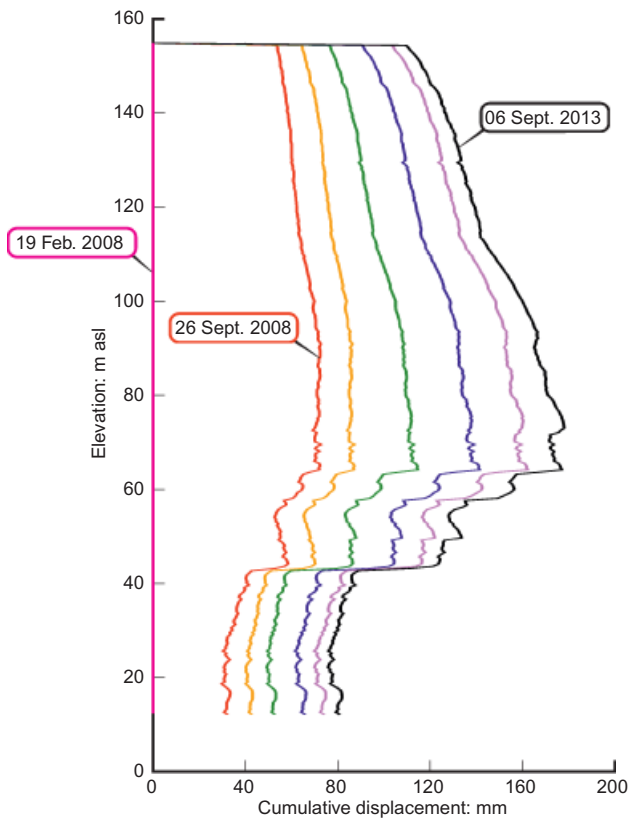


Fig. 16. East dam, response of deep inclinometer located on the dam

in the region of cross-section XVIIIE, the following stabilisation measures were implemented.

- Construction of a stabilisation berm at the toe of the dam. In view of the observed mechanics of the movement, the effectiveness of the berm is mostly controlled by the residual shear strength ($6.5^\circ < \phi'_r < 8^\circ$) available on the glacio-tectonic shear surface on which most shear displacements occur.
- Relocation of the dam crest 150 m towards the pond. This remedial measure was implemented when the dam crest was at 165 m asl; it only became effective after further impounding above this elevation (see Fig. 17).
- Drilling of 20 relief wells, 105–150 m deep, located at the starter dam and on the side-slopes of the dam, at elevations up to 165 m asl. These wells are screened over the entire thickness of the Pliocene deposits to intercept any



Dam crest moved 150 m towards pond

Fig. 17. East dam, relocation of dam crest

pervious horizons encountered in the wells. The discharge of the 14 wells in the region of cross-section XVIIIE (measured once continuous pumping started in 2008) varies considerably between $0.5 \text{ m}^3/\text{day}$ and $8 \text{ m}^3/\text{day}$, with a trend to decrease slowly with time.

Four other wells were installed close to section XVIIIE, and another close to cross-section XVIIIE. Since mid-2012 the discharge from individual wells has varied between $0.1 \text{ m}^3/\text{day}$ and $4.0 \text{ m}^3/\text{day}$. This range of well discharge reflects the complexity of the local geology, with the efficiency of the relief wells depending on the continuity of the pervious horizons and their contrast with the very low permeability ($k < 1 \times 10^{-9} \text{ m/s}$) of the Pliocene clay.

The stabilisation measures described above were implemented during 2007–2009. In spite of some doubts regarding the precise mechanisms involved, the stabilisation of the East dam has been effective, resulting in a reduction of movement measured on the starter dam of between 10 mm/year and 15 mm/year, about one third of the rate observed previously (see Fig. 13 and Table 1).

The response of 32 selected vibrating wire piezometers located in the area influenced by the relief wells allows the following tentative conclusions. Since commencing the installation of the relief wells in mid-2008, although most of the vibrating wire piezometers show a trend of either reduced or constant pressures, some piezometers display increasing pore pressures. During this period the dams have increased in height by 1 m to 1.5 m per year, which will have increased the stresses on the foundation soils; the increased pore pressures are therefore presumably the result of local stress increases experienced by the piezometers. Other uncertainties are linked to the considerable spatial variability of the foundation soils, which makes it almost impossible to know the location of each piezometer with respect to the drainage boundaries. Table 2 shows the response of 14 East dam piezometers located between cross-sections XIVE and XVIIIE where the relief wells are in use, showing those with the most significant decrease of pore pressure (DiBiagio & Strout, 2013). This table gives the elevation of the static ground water level at natural ground level prior to dam construction, and thus indicates the excess pore pressure due to dam construction. Each piezometer has its filter embedded in Pliocene clay.

Figure 18 shows examples of three vibrating wire piezometers which are responding to two nearby relief wells. Despite the complex stratigraphy of the Pliocene sediments it can be seen that these piezometers provide encouraging examples of the effectiveness of the relief wells in reducing the excess pore pressure under the dam. Regardless of all the uncertainties linked to the random response of the wells in terms of their yield, and of the piezometers in terms of the pore pressure changes with time, the reduction of the displacement rate of the East dam can probably be largely ascribed to the operation of the relief wells.

North dam

Although only about half as high as the East dam, the North dam (original ground level between 137 and 141 m asl; stated dam elevation $\approx 145 \text{ m asl}$, ground water table 3–5 m deep) started exhibiting horizontal displacements in 2006/2007, a trend that has increased with time. Fig. 19 shows the movements of the northern starter dam since 2008. These displacements are localised along two lengths of the dam between cross-sections VaN-IXN and XIVN-XIXN. The intervening length of dam, near cross-section XN, is subject to much smaller movements. Fig. 20 shows the history of the North Dam construction, together with the

Table 2. East dam – response of 14 vibrating wire piezometers to relief wells operations according to NGI report by DiBiagio & Strout (2013)

Cross-section	Piezometer	Groundwater level elevation: m asl	Filter elevation: m asl	Δu : kPa	
XVIII E	7A	168.4(D)	60.4	-200	Pliocene clay
XVIII E	7B	168.4(D)	81.4	-120	Pliocene clay
XVIIIa E	1A/1	157.7(D)	66.7	-100	Pliocene silty clay
XVIIIa E	1A/2	157.7(D)	66.7	-100	Pliocene silty clay
XVIII E	1A	166.3(D)	37.3	-80	Pliocene clay
XVII E	5B/2	136.6(SD)	85.6	-40	Pliocene silty clay
XVII E	5B/2	115.3(SD)	89.3	-40	Pliocene silty clay
XVIIIa E	2B/1	136.6(D)	85.6	-30	Pliocene clay
XVII E	6A/1	115.3(SD)	41.3	-30	Pliocene clay
XVII E	6A/2	115.3(SD)	41.3	-30	Pliocene clay

Note: Original ground level elevation: 116 m asl; starter dam elevation: 135 m asl; groundwater level, depth 1 m to 3 m below ground level; (D) = dam; (SD) = starter dam.

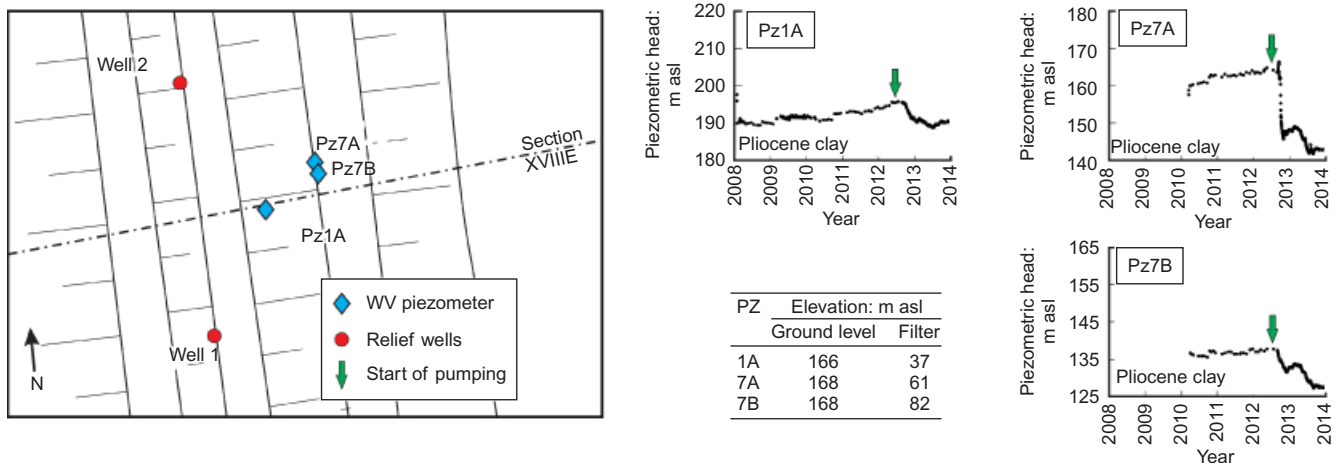


Fig. 18. East dam, cross-section XVIII E: example of vibrating wire piezometers response to relief wells operation (adapted after DiBiagio & Strout (2013))

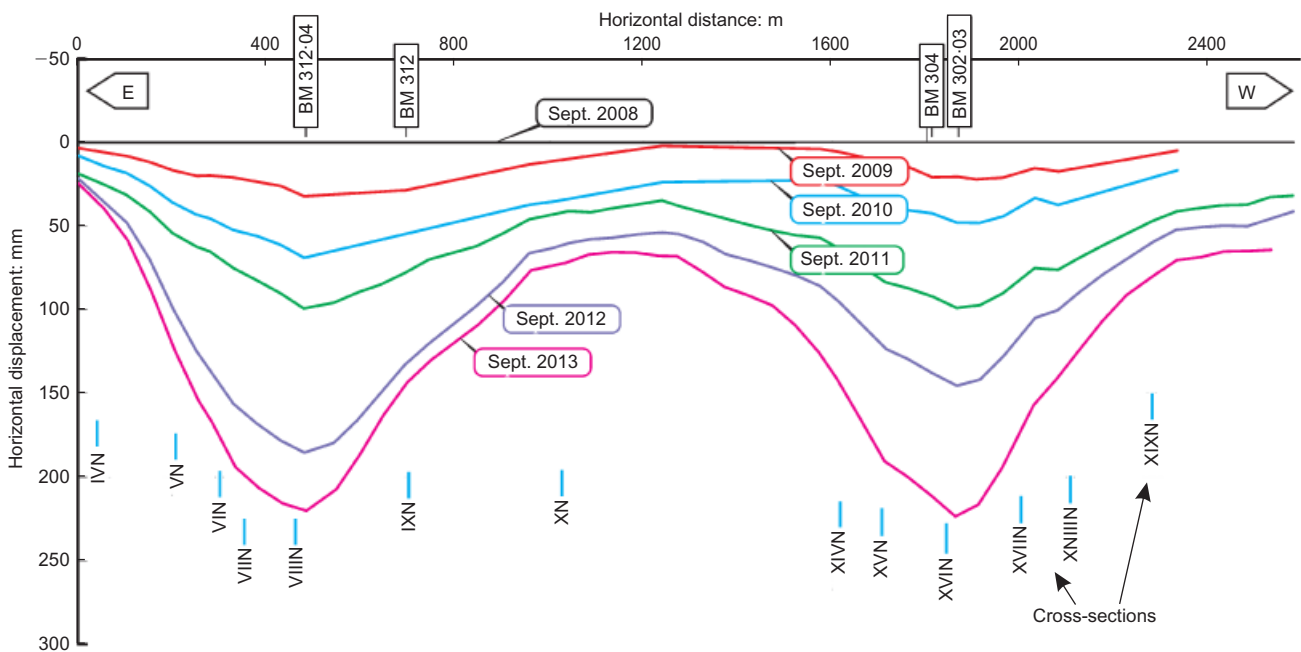


Fig. 19. Northern starter dam: plan view of horizontal surface displacements

time history of horizontal displacements of BMs 304 and 312, located on the starter dam, from 1987.

Table 3 summarises the horizontal surface displacement during the period 2010–2013 for the two benchmarks shown in Fig. 20. During the same period the corresponding

displacements (and the displacement rates) of cross-section IXN (Fig. 19) remain lower than those of adjacent cross-sections VIIIN and XVIN, although with a slight trend to increase with time.

Unlike the East dam, the horizontal displacements of the

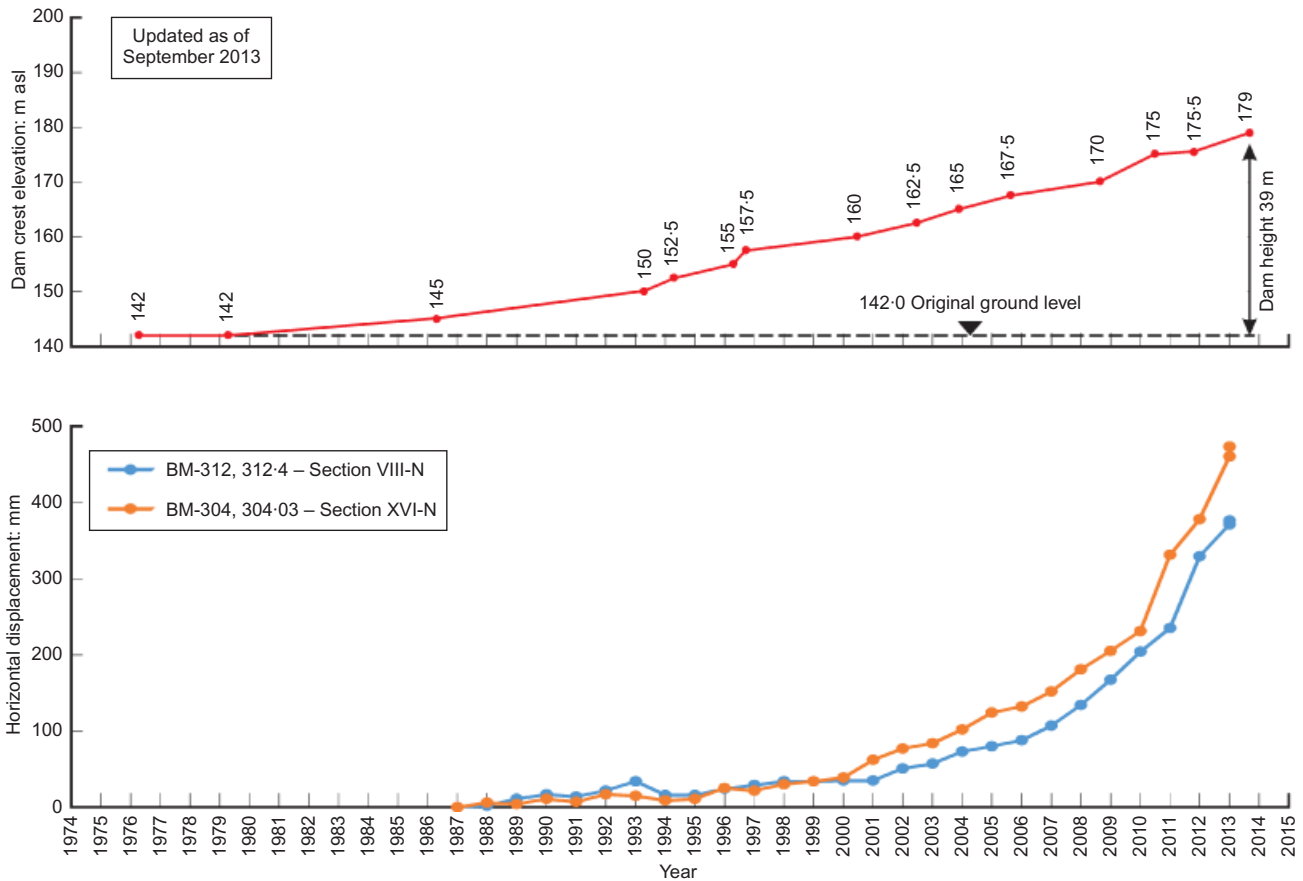


Fig. 20. Cross-sections VIII-N and XVI-N: construction history and horizontal surface displacements

Table 3. North dam horizontal surface displacements rates of benchmarks quoted in Fig. 20

Section VIII-N		Section XVI-N	
mm/year	Year	mm/year	Year
32.9	2008–2009	27.9	2008–2009
22.0	2009–2010	21.8	2009–2010
29.7	2010–2011	51.7	2010–2011
90.0	2011–2012	38.0	2011–2012
41.0	2012–2013	83.0	2012–2013

Note: Total displacements (section VIII-N) from 1987 to December 2013: 283 mm; total displacements (section XVI-N) from 1987 to December 2013: 408 mm.

North dam are accompanied by heave of the crest of the starter dam and of the adjacent area downstream of the dam toe (see Fig. 21), which in correspondence with the cross-section VIII-N, at the end of 2012, reached 66 mm. The geodetic surveys carried out in 2013 suggest that the rate of heave of cross-section VIII-N has reduced to a few mm/year or has even ceased, while cross-section XVI has maintained a rate of about 9.5 mm/year, where the total heave is, however, smaller, about 35 mm. Table 3 gives the impression that the movements of cross-sections VIII-N and XVI tend to alternate with time, which displays the greater displacement rate. However, the results of the inclinometer measurements given in Fig. 22 (inclinometers 16a-N-7A and 7N-7A), show that the horizontal displacements at depth on the glacio-tectonic shear planes are greater than those measured at the starter dam. This trend is common to all ten inclinometers located in the area of cross-sections VIII-N and XVI-N (see Table 4).

The inclinometer data shown in Fig. 22 indicate that neither inclinometer casing is fixed at the toe, which is typical for all inclinometers in the East and North dams. As stated earlier, all inclinometers have been interpreted using the ‘top-down’ approach.

Both Table 4 and Fig. 22 demonstrate that the mechanism of the movements of the North dam is different and more complex than that of the East dam. Although horizontal displacements occur on glacio-tectonic shear planes, the inclinometers indicate that there is also rotational movement. This is consistent with the data in Table 4, which show that the horizontal movement of the top of the inclinometers is less than at the depth of the active glacio-tectonic shear planes. This trend is more pronounced for inclinometers installed within the dam at higher elevations, compared to those in the starter dam.

As a consequence of the high displacement rates of the North dam, and the observed heave of the starter dam, stabilisation measures are presently being implemented. In view of the positive response of the East dam to remedial measures, similar stabilisation measures have also been adopted for the North dam.

In 2012 the crest of the entire length of the North dam, then at elevation of 175 m asl, was realigned 100 m inwards towards the pond. Of the 36 relief wells planned as remedial measures for the North dam, six have already been installed, three near cross-section VIII-N, and three in the region of the cross-section XVI-N. These wells have been in operation since March 2013. The remaining relief wells will be installed and brought into operation over the next 12–18 months. The small number of wells, and the limited time over which they have been in operation, has not yet had an effect on the movements of the North dam, although a few of the vibrating wire piezometers are exhibiting a reduction in pore pressure.

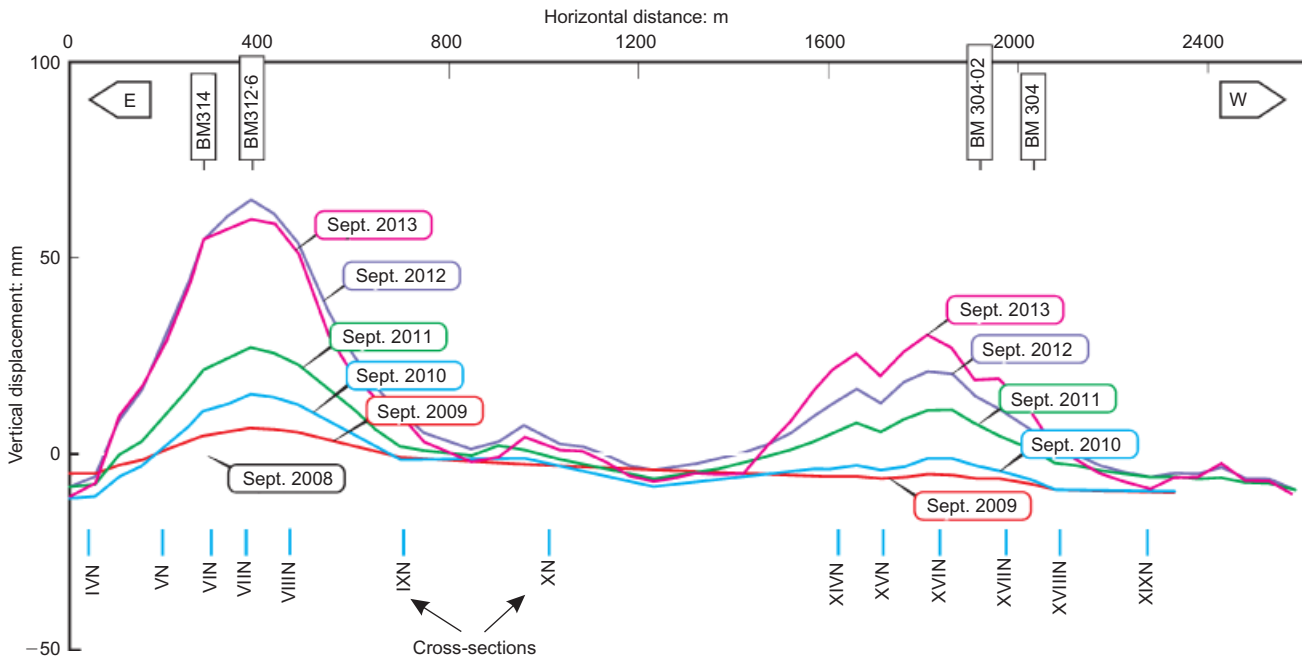


Fig. 21. Cross-sections VIIIIN and XVN: heave of the northern starter dam, benchmarks (BMs) 314, 312-06, 304, 304-03

The discharge rate given by the wells is as random as experienced at the East dam, ranging between about $0.5 \text{ m}^3/\text{day}$ and $4 \text{ m}^3/\text{day}$.

Because of the intensity of the glacio-tectonic disturbance experienced by the dam foundation, the success of the stabilisation measures at the North dam cannot be taken for granted.

In comparison with the behaviour of the East dam, a period of at least 12–18 months may be necessary before a reduction of the displacement rate is observed, the only criterion that can be used to assess the effectiveness of the stabilisation measures. Given the behaviour of the East and North dams it is worth recalling a statement by Hutchinson (1995): ‘In any stability problem the most important question is generally whether or not pre-existing discontinuities, especially shears, are present.’ The behaviour of the Zelazny Most ring dam is an excellent example that confirms fully the wisdom of this statement. Since KGHM intend to raise the ring dam to provide eventual further storage capacity of about $500 \times 10^6 \text{ m}^3$ of tailings until the ore body is exhausted in 25–30 years, the Zelazny Most development strategy needs to be carefully re-examined.

GEOTECHNICAL SITE CHARACTERISATION

Foundation soils

The characterisation of the foundation soils considered here refers mainly to the East dam, where movement was first observed. A representative soil profile is exhibited by cross-section XVIIE as shown in Fig. 10. The upper strata are of mainly sandy deposits, with a combined thickness of about 10 m. Below, well beyond the maximum depth explored of about 100 m, are Pliocene deposits, consisting mainly of fresh water medium to very high-plasticity clay. As previously stated, the extreme spatial variability of the Pliocene sediments makes it very difficult to develop a satisfactory geotechnical model.

For this reason, the soil investigation was carried out downstream of the dam, more than 100 m downstream from the toe of the starter dam, to ensure that laboratory and in-situ test results were not affected by the presence of the dam. Undisturbed samples were retrieved from a series of

boreholes drilled to depths between 90 m and 100 m, and were sent to three geotechnical laboratories: Geoteko (Warsaw, Poland), Ismgeo (Bergamo, Italy) and Norwegian Geotechnical Institute (NGI, Oslo, Norway). The following tests were carried out, concentrating on the Pliocene clay

- index properties and grading curves
- in-situ stress state
- shear strength: undrained (not discussed here), drained and residual strength tests
- stress–strain–time behaviour.

Figures 23–26 summarise the results of the index properties and grading of the clay samples. The ranges of the depth over which the inclinometers indicate the presence of glacio-tectonic shear planes are indicated.

Figure 23 reports the variation of the bulk unit weight, γ_t with depth, which ranges between 20.5 kN/m^3 and 22.0 kN/m^3 . Somewhat lower values, 19.5 kN/m^3 to 20.0 kN/m^3 , are found within the zones containing intensely slickensided clay.

The specific gravity, G_s , of the Pliocene clay, is 2.70 ± 0.02 . The clay fraction (CF) varies as a function of w_l and typically falls in the following ranges: for $w_l < 70\%$, $CF = 50 \pm 12\%$, and for $w_l > 70\%$, $CF = 66 \pm 15\%$. Fig. 24 shows the values of the natural water content w_n , together with the values of the Atterberg limits.

In spite of the scatter, the data shown in Fig. 24 seem to suggest that the zones containing intensely slickensided clay layers are characterised by fairly high values of w_n (e.g. Skempton & Petley, 1967) and very high values of w_l . This is particularly evident in the deeper slickensided zone, which is the most active shearing plane under the East dam. Fig. 25, shows that the values of liquidity index (LI) vary between 0.0 and -0.2 , and that the values of clay activity (A_c) range between 1.0 and 1.4. To complete the review of the index properties, Fig. 26 shows the variation of initial void ratio, e_0 , of the Pliocene clay, which ranges between 0.40 and 0.75. Again, note that there is a concentration of higher values in the zones of intensely slickensided layers.

With respect to the degree of saturation, the clay can be regarded as fully saturated ($S_r = 1$), the values >1.0 resulting from measurement errors in the values of w_n and/or G_s .

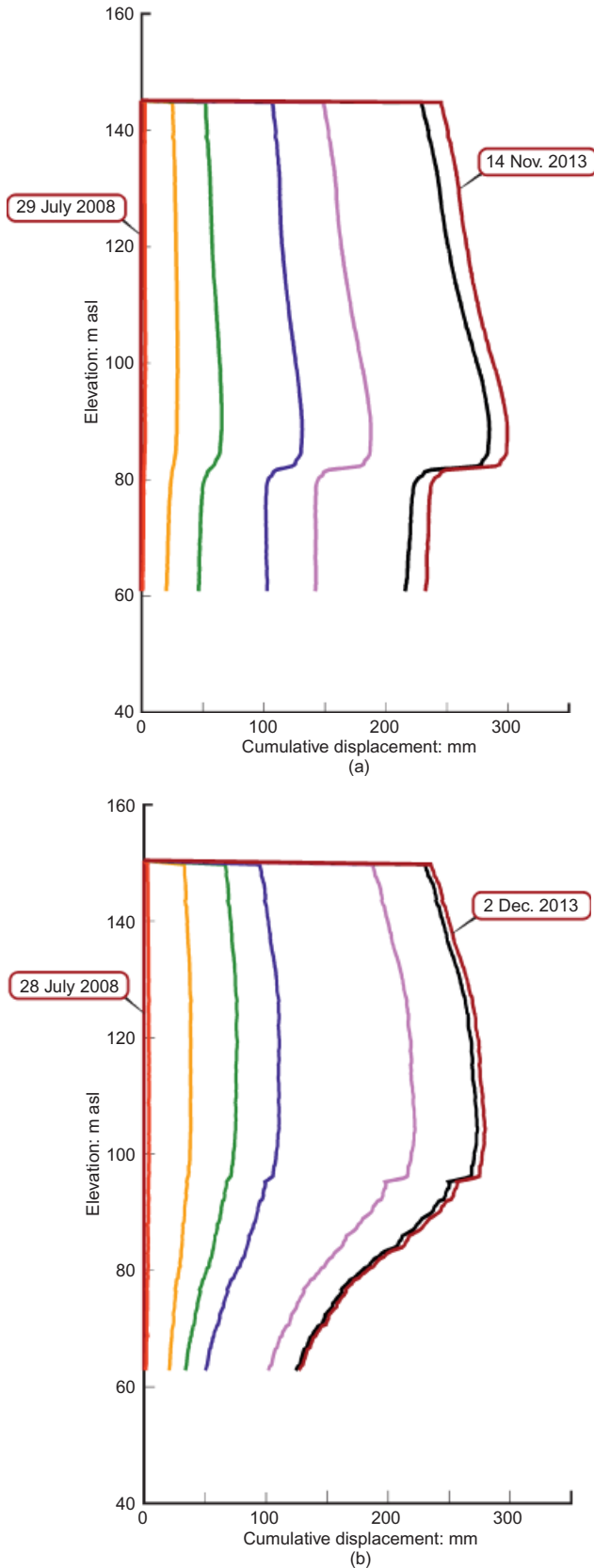


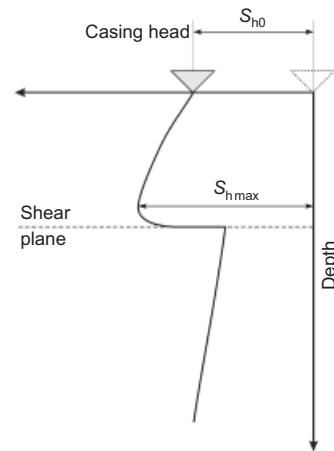
Fig. 22. Northern starter dam, response of deep inclinometers: (a) 16aN-7 A; (b) 7N-7 A

Permeability of the Pliocene clay. Figure 27 reports the values of the coefficient of permeability, k , deduced using the empirical correlation approach of Feng (1991). However, since there are randomly spaced sandy and gravelly layers of variable extent in the Pliocene clay, these laboratory values of

Table 4. Response of inclinometers on the North dam

Incl. no.	Head: m asl	Toe: m asl	Shear plane:* m asl	$s_{h\max}/s_{h0}$
Starter dam:				
5aN-7	145	57	98	1.07
5aN1-9	145	85	113	1.08
9N1-9	146	52	67	1.43
16N-7	146	82	89	1.22
16aN7	146	60	80	1.29
Dam:				
5aN-8	165	65	74	2.31
7N-7	151	95	62	1.92
9N2-9	160	68	82	1.43
16aN-8	165	65	91	1.74
9N4-10	178	49	120	2.78

* Active shear plane.



Note: s_{h0} = inclinometer head horizontal displacement; $s_{h\max}$ = maximum displacement at shear plane elevation.

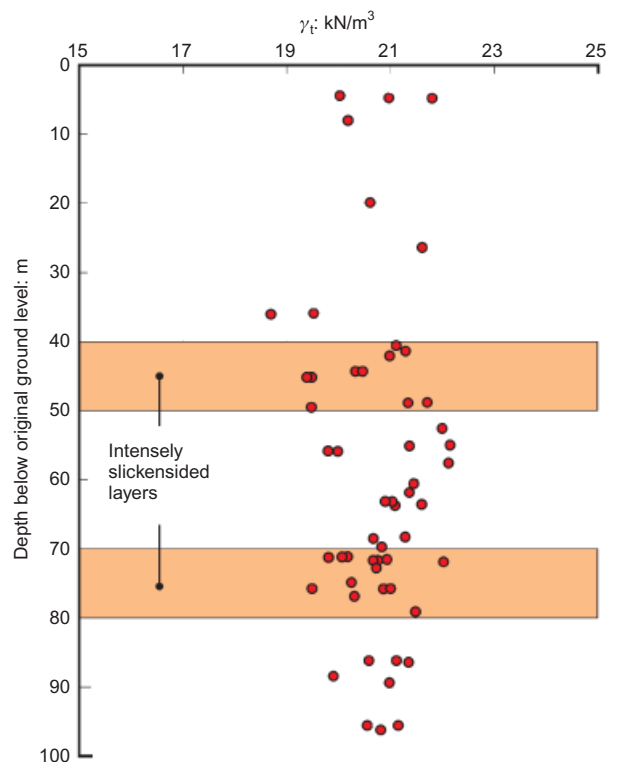


Fig. 23. Pliocene clay: bulk unit weight

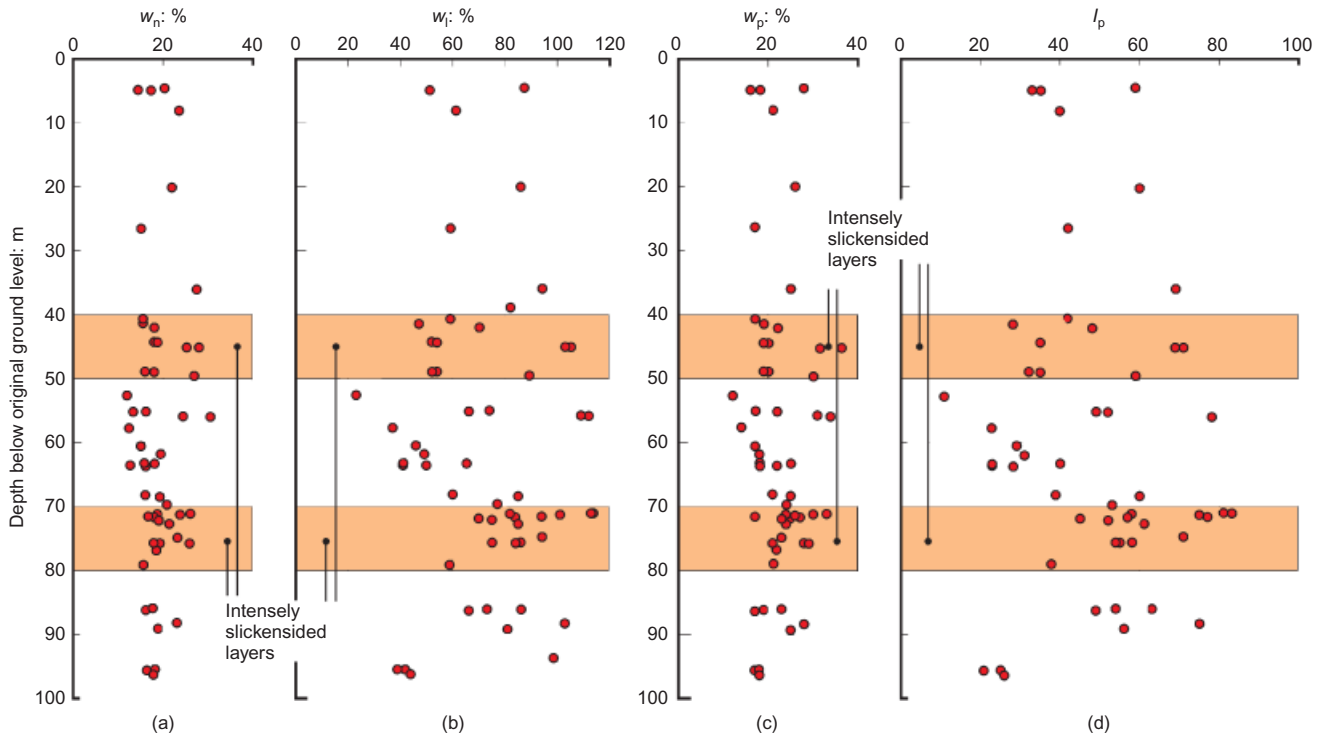


Fig. 24. Pliocene clay: water content and Atterberg's limits: (a) natural water content; (b) liquid limit; (c) plastic limit; (d) plasticity index

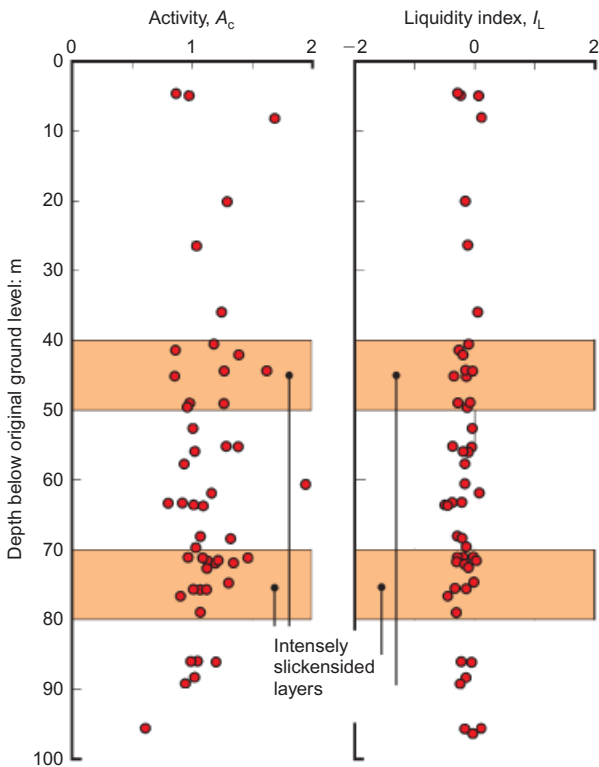


Fig. 25. Pliocene clay: activity and liquidity index

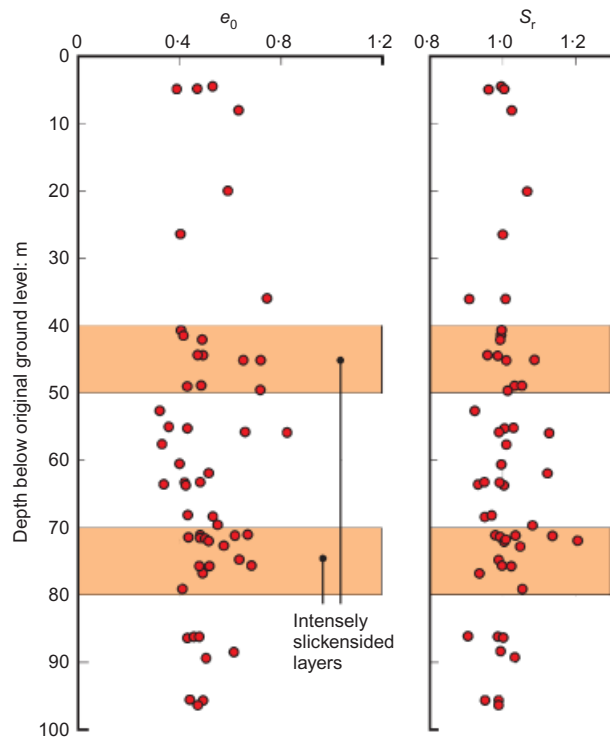


Fig. 26. Pliocene clay: void ratio and saturation degree

k do not represent the bulk permeability of the foundation soils at the field scale. The bulk value of k in the field is certainly higher than the laboratory values. Consequently the extreme spatial variability of the soils at Zelazny Most makes any in-situ or large-scale laboratory tests difficult to carry out and of only local validity.

This conclusion is supported by the observed randomly variable discharge from the relief wells, and by the variable

pore pressure measurements. For these reasons the assessment of equivalent field scale k values was made by trial and error procedure, using a coupled effective stress consolidation finite-element analysis (FEA). In this analysis the best estimate of field equivalent k was taken as that which gave the best fit to the observed horizontal displacements and excess pore pressure measured in cross-section XVIE.

The range of field scale results, also given in Fig. 27, can be, to a first approximation (at least for cross-section XVIE),

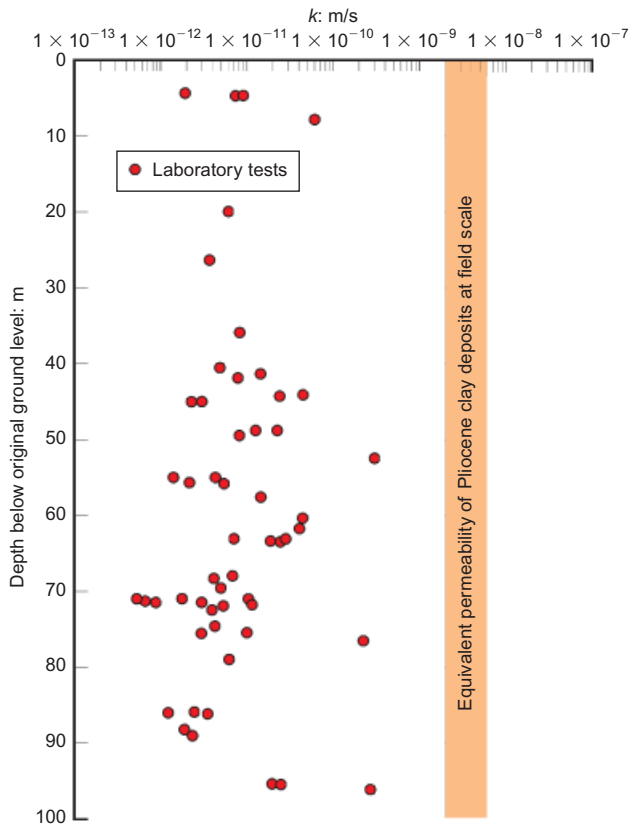


Fig. 27. Pliocene clay: permeability coefficient

regarded as the ‘equivalent’ bulk coefficient of permeability for the Pliocene deposits, obtained as described above.

In-situ initial state and stress history. This is examined using the results of tests on undisturbed specimens of the Pliocene clay. Fig. 28 shows the in-situ initial state of the tested specimens, plotted in terms of effective overburden stress (σ'_{v0}) and void index I_v (Burland, 1990).

The same figure also shows the intrinsic compression line (ICL_{oed}), the one-dimensional compression curve for reconstituted normally consolidated clay; that is, a clay that has neither sensitivity nor bonding (Skempton & Hutchinson, 1969; Burland, 1990; Cotecchia & Chandler, 1997; Chandler, 2000, 2010).

As will be seen, all the undisturbed samples exhibit an initial in-situ state well below the ICL_{oed} (see Fig. 28). This condition, together with the low values of k , the negative values of LI and the lack of bonding, is conducive to high-quality undisturbed sampling, thanks to dilation generating

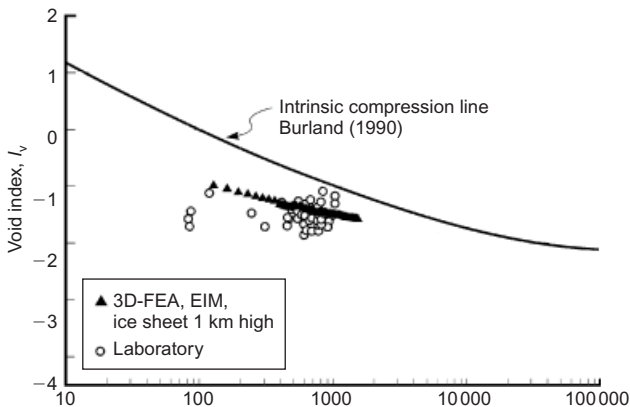


Fig. 28. Undisturbed samples of Pliocene clay: in-situ state

high negative pore pressures upon removal of the in-situ total stresses when sampling.

Figure 28 also shows the initial in-situ state of the Pliocene clay at the end of melting of the ice sheet (EIM), as simulated in the FEA. The FEA simulation generates in-situ states, which are in agreement with the laboratory tests. The results of this analysis are discussed in the next section.

An example of the suctions measured in the Pliocene clay, using the Ridley and Burland suction probe (Ridley & Burland, 1993, 1995), is shown in Fig. 29, taken from Chandler *et al.* (2011). The measurements were made in a field laboratory shortly after sampling, on selected clay samples lacking any significant amount of silt. The favourable conditions for sampling enabled an assessment of the coefficient of earth pressure in Pliocene clay using these suction measurements.

The evaluation of the coefficient of the earth pressure at rest ($K_0 = \sigma'_{h0}/\sigma'_{v0}$) based on suction measurements originates from Skempton (1954). Assuming that the soil is isotropic, elastic and fully saturated, and assuming that Skempton’s pore pressure coefficient A_S is 1/3 (Skempton, 1954), K_0 can be computed by means of the following formula.

$$K_0 = (3p_k - \sigma'_{v0})/2\sigma'_{v0}$$

where p_k is the measured suction, σ'_{v0} is the effective vertical stress, and σ'_{h0} is the effective horizontal stress.

The values of p_k measured on the Pliocene high-plasticity clay samples, ignoring the samples containing silty lenses,

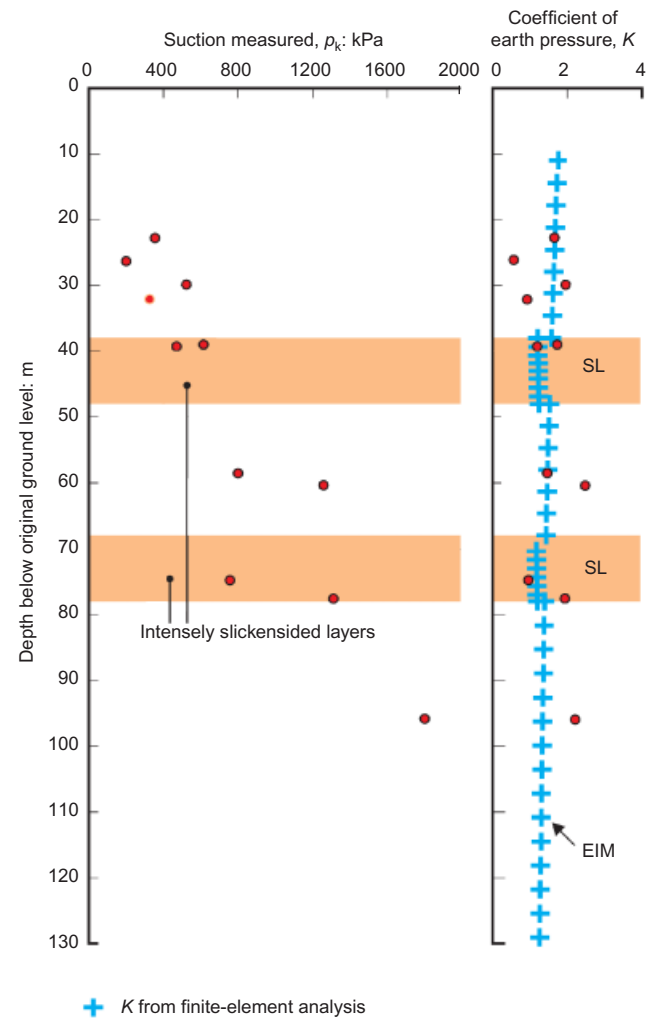


Fig. 29. Measured p_k and computed K values (SL: intensely slickensided layers; EIM: end of ice melting (FEA))

are shown in Fig. 29. Also shown in Fig. 29 are the values of K inferred from the FEA at EIM. The symbol K is used rather than K_0 as the Pleistocene ice sheets will have imposed a stress state akin to simple shear to the foundation soils. This implies that radial stress symmetry in the ground is very unlikely, so the symbol K_0 is inappropriate.

The stress history of the Zelazny Most foundation clays can reasonably be modelled as a mechanically overconsolidated clay, subjected in the past to a maximum vertical effective stress $\sigma'_{v\max}$, considerably higher than the current σ'_{v0} . Based on geological evidence it can be postulated that during the Pleistocene the foundation soils at Zelazny Most were subject to at least three cycles of ice sheet transgression and subsequent melting. The thickness of the ice sheets probably ranged between 800 m and 1200 m. In the following, neglecting the effect of the several loading–unloading cycles to which the Pliocene sediments must have been subject in the past, it is assumed that there was a single ice advance, which provided a maximum effective overburden stress $\sigma'_{v\max} = 10$ MPa, equivalent to an ice sheet thickness of 1000 m.

Shear strength. The development of the Zelazny Most depository is an on-going construction project, with frequent analyses of the stability and displacements of the dams, both with limit equilibrium and finite-elements methods. These analyses have to be carried out in terms of effective stresses, whereby the drained soil strength is of primary interest, in conjunction with the pore pressures measured in the field. For these reasons the following is limited to discussion of the results of drained triaxial compression and extension tests on undisturbed samples, and of drained ring-shear tests carried out on reconstituted clay specimens in the Imperial College–NGI apparatus.

The undisturbed samples were obtained using a double-tube rotary core sampler with an internal spring-loaded cutting shoe. The samples had a diameter of 80 mm, and a length between 600 mm and 800 mm, from which triaxial

specimens were trimmed to 50 mm in diameter and 100 mm high.

The triaxial test types used were

- (a) isotropically consolidated, drained compression tests (TX-CID-C)
- (b) isotropically consolidated drained extension tests (TX-CID-E).

The specimens were reconsolidated to the best estimate of the in-situ mean effective stress (p') with K in the range of $1.5 \leq K \leq 1.7$ as obtained from the suction measurements (Fig. 29).

Figures 30 and 31 summarise the results of the TX-CID-C and TX-CID-E tests respectively. Figs 32 and 33 show the stress–strain curves in compression and extension typical of very high-plasticity ($w_l \geq 70\%$) destructured clay. In compression there is very limited strain-softening. The stress–strain curves of the extension tests do not show any deviatoric stress decrease after reaching peak.

This conclusion does not entirely apply to the results of triaxial tests carried out on clay specimens of medium to high-plasticity clays ($w_l < 70\%$). These samples contain only small slickensides, and apparently do not have any significant shear planes; in the following discussion such samples will be referred to as ‘bulk’ clay.

Stress–strain curves for the bulk clay, again with TX-CID-C and TX-CID-E tests, are shown in Figs 34 and 35. In this case, curves from compression tests show slightly more post-peak strain-softening than do the high-plasticity clays, while the extension test curves do not show any sign of deviatoric stress decrease after reaching peak.

Figure 36 summarises the effective stress peak friction angle ϕ' as a function of w_l obtained from triaxial tests on undisturbed samples of Pliocene clay taken downstream of the toe of the East dam. These have been interpreted assuming that, due to the glacio-tectonic disturbance suffered by the clay, the Mohr–Coulomb strength envelope has an effective stress cohesion intercept $c' = 0$. This disturbance

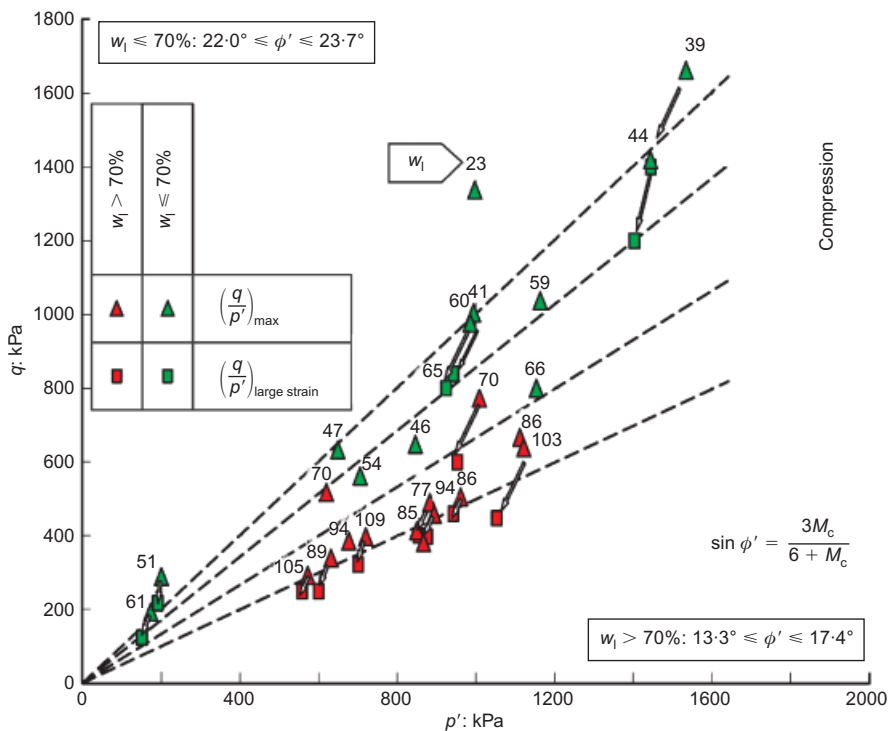


Fig. 30. Drained shear strength from drained triaxial compression test on isotropically consolidated specimen (TX-CID-C) tests

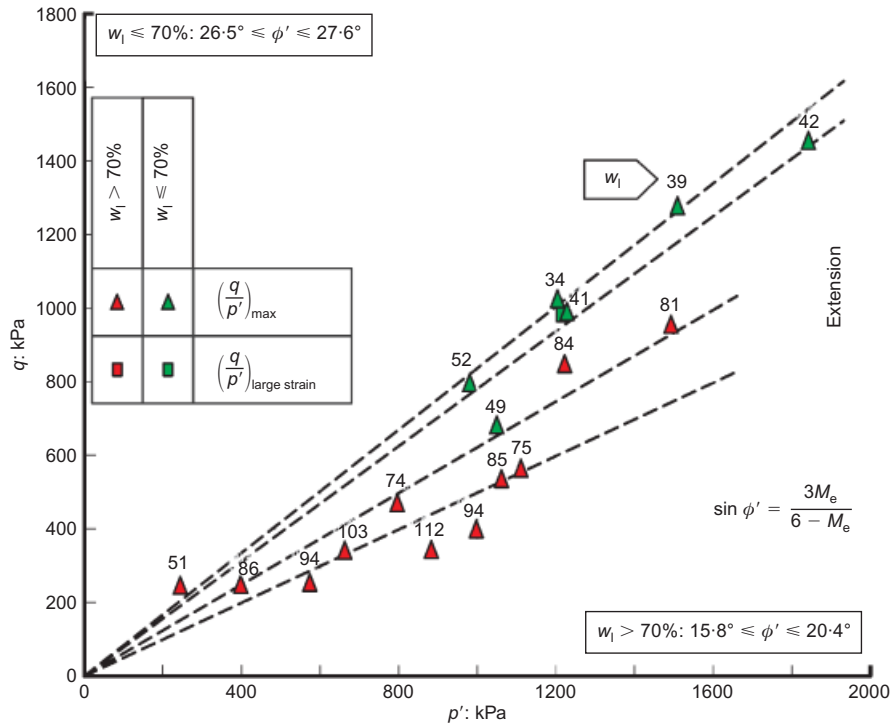


Fig. 31. Drained shear strength from drained triaxial extension test on isotropically consolidated specimen (TX-CID-E) tests

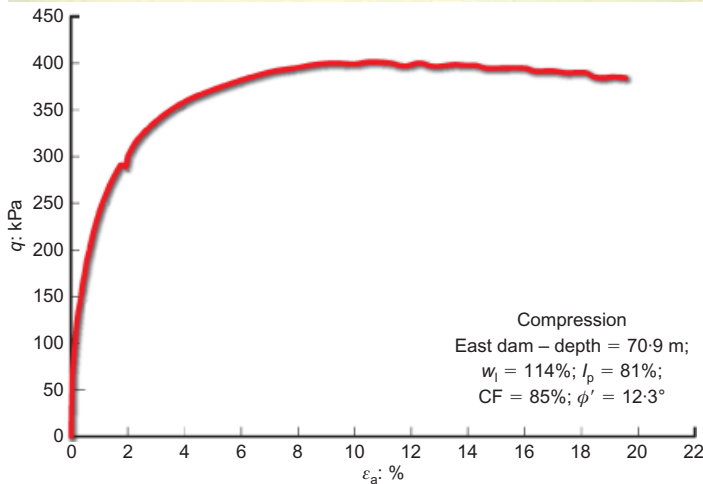


Fig. 32. Stress–strain curve of very high plasticity clay from TX-CID-C tests

has affected the Zelazny Most Pliocene sediments in two ways

- (a) by inducing enormous shear forces to depths of at least 100 m during the ice advance
- (b) by subjecting the Pliocene clay during the various glaciations to several vertical stress load–unload cycles in the range ± 10 MPa, so that swelling during and after ice melting will have changed significantly both the mechanical characteristics and the in-situ stress state of the Pliocene clay (Chandler, 2010).

Both these phenomena will have destroyed the original structure of the Pliocene clay, triggering, particularly under large overburden stresses, a high degree of face-to-face alignment of the platy clay particles along the direction of shear, which is particularly pronounced in very high-plasticity clays (Morgenstern & Tchalenko, 1967; Skempton & Petley, 1967; Lupini *et al.*, 1981; Skempton, 1985; Burland *et al.*, 1996; Anantanasakul *et al.*, 2012).

For these reasons the range of ϕ' values for clays with $w_l \geq 70\%$ (Table 5) is significantly lower than those at the critical state ϕ'_{cv} , which relate to unstructured, mechanically

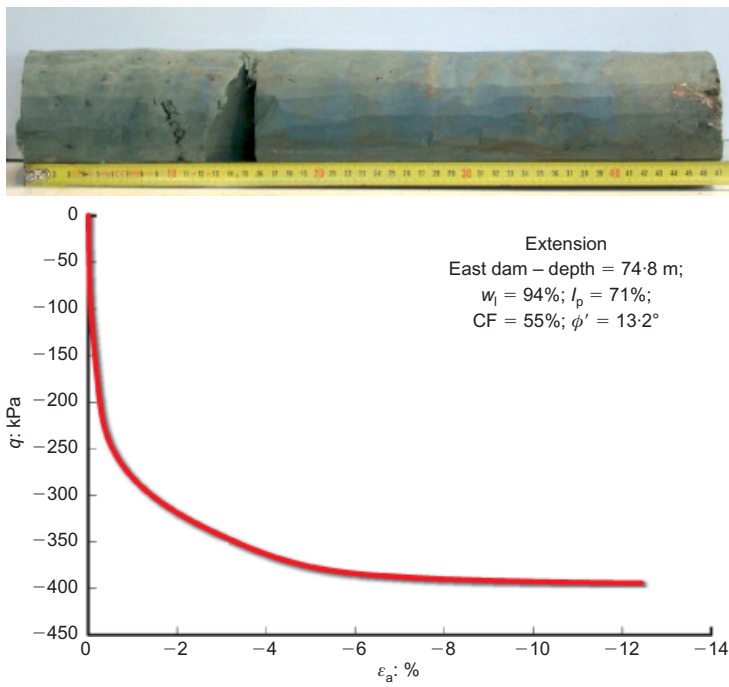


Fig. 33. Stress-strain curve of very high plasticity clay from TX-CID-E tests

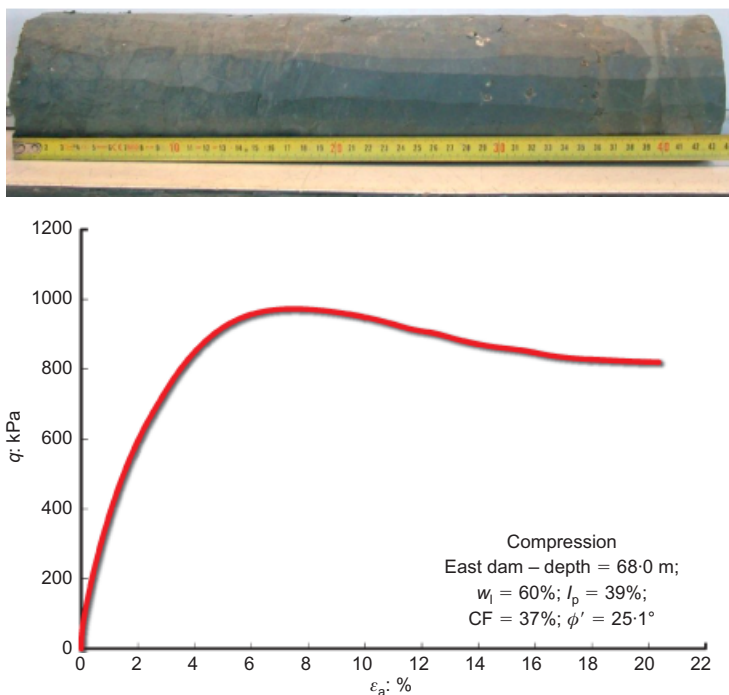


Fig. 34. Stress-strain curve of high plasticity clay from TX-CID-C tests

overconsolidated clays of comparable plasticity. The lower plasticity clays ($40\% \leq w_1 < 60\%$) are similarly affected, although less dramatically, as also seen in Table 5. In this case, the upper bound of ϕ' values at the peak falls between 22° and 26° , equal to or slightly lower than ϕ'_{cv} of unstructured clays with comparable plasticity.

The residual shear strength (Skempton & Hutchinson, 1969; Lupini *et al.*, 1981; Skempton, 1985; Wedage *et al.*, 1998; Georgiannou & Burland, 2001; Toyota *et al.*, 2009) was assessed at Imperial College London and at NGI using drained multi-stage ring-shear tests. The ring-shear specimens were consolidated under vertical stresses between 150 kPa and 1000 kPa, and cover the range of w_1 from 70%

to 100%. The residual friction angle (ϕ'_r) values are summarised in Fig. 37.

The use in design of ϕ'_r from ring-shear tests is not directly applicable at Zelazny Most. The reasons for this are given below.

- (a) At both East and North dams the horizontal movement along the glacio-tectonic shear planes occurs at 90° and 180° , respectively, to the approximate north-south direction of the ice sheets during the Pleistocene. It seems likely that, where the direction of movement on pre-existing shear planes has changed, a higher value of

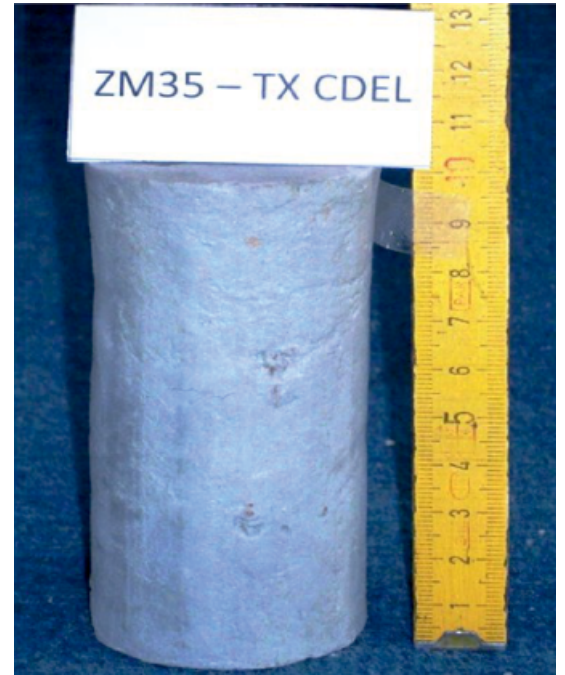
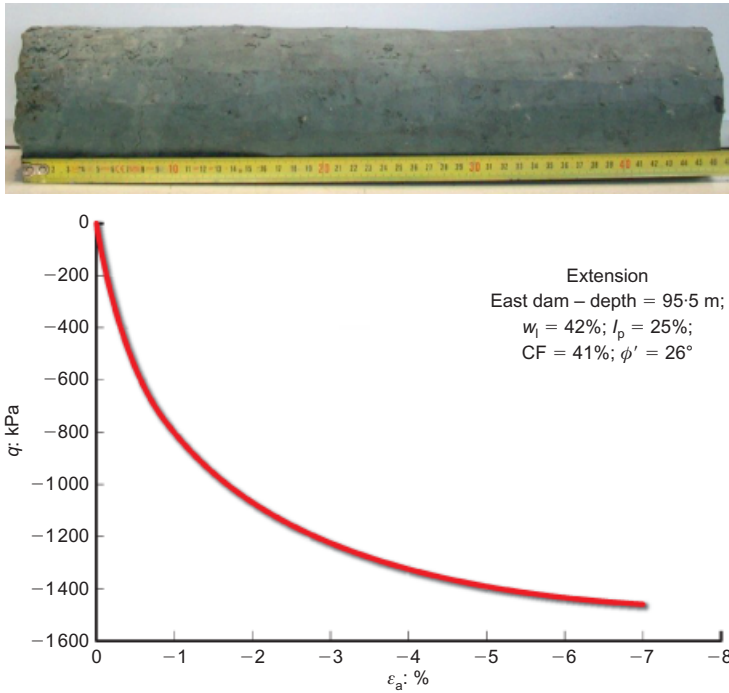


Fig. 35. Stress-strain curve of medium plasticity clay from TX-CID-E tests

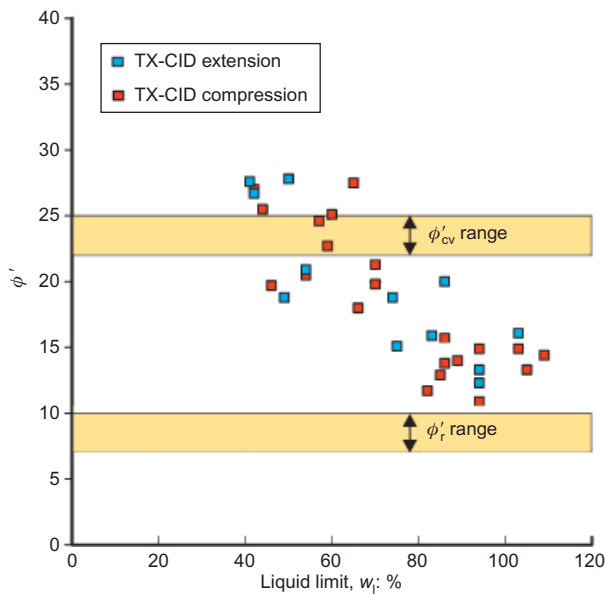


Fig. 36. Summary of the drained triaxial tests results

ϕ' than ϕ'_r will be mobilised, at least until substantial displacement has occurred in the 'new' direction.

- (b) It has been known for some time that when existing landslides are re-activated, the shear strength (ϕ' , $c' = 0$) inferred from back analysis is often somewhat higher than measured in the ring-shear apparatus; see for

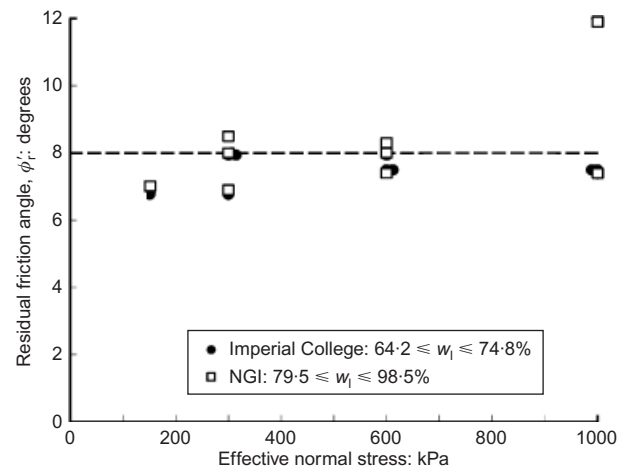


Fig. 37. Residual shear strength: tests in ring shear apparatus

example Chandler (1977) and Gibo *et al.* (2002). For similar reasons it is presumed that values of ϕ' relating to extensive glacio-tectonic shear zones will also be larger than the ring-shear value of ϕ'_r .

The FEA discussed in the following section considers only the effects of a single ice sheet advance on the shear strength. The finite-element simulation, however, shows that a single cycle of ice melting is enough to reduce the mobilised bulk value of ϕ' of the intensely slickensided

Table 5. Range of triaxial tests results in terms of M value and ϕ'_{peak} at failure

w_1 : %	TX-CID-C		TX-CID-E	
	M_c^*	ϕ'_c : degrees	M_c^*	ϕ'_c : degrees
$\geq 70\%$	0.427 ÷ 0.664	13.3 ÷ 17.4	0.499 ÷ 0.625	15.8 ÷ 20.4
$< 70\%$	0.857 ÷ 0.928	22.0 ÷ 23.7	0.777 ÷ 0.802	26.5 ÷ 27.6

* For the meaning of M_c and M_e see Figs 31 and 32, respectively.

plastic clay ($w_1 \geq 70\%$), from peak ($22^\circ \leq \phi'_{cv} \leq 24^\circ$, $c' = 0$), to values ranging between 9° to 11° .

Stiffness at small strains. The shear modulus of the Pliocene sediments at very small strains, G_0 , including slickensided layers, was measured in situ using shear wave velocities (V_s) in advanced cross-hole tests (CHT) at locations downstream of the toe of cross-section XVIE [(Jamiolkowski, 2012; Callerio *et al.*, 2013)], as shown in Fig. 38.

Moreover, V_s was also measured in the laboratory, using bender element tests, on the same undisturbed specimens as used for triaxial tests. The values of V_s obtained from these tests were, where appropriate, corrected to account for the differences between the mean effective consolidation stress imposed in the laboratory and the best estimate of the mean effective stress at the depth of sampling.

It will be seen that the values of V_s resulting from the bender elements compare fairly well with those in the field cross-hole tests. This comparison, considering the geological setting and the in-situ initial state (see Fig. 28), suggests that the Pliocene clay in situ is destructured, with no or negligible bonding between particles.

According to the classification proposed by Rocchi *et al.* (2012, 2013) the Zelazny Most Pliocene clay can be classified as mechanically overconsolidated, with an initial state located below the oedometer intrinsic compression line (ICL_{ocd}), defined by Burland (1990).

Tailings

Since the commencement of their involvement in the Zelazny Most project in 1992 the IBE has routinely paid special attention to the geotechnical characterisation of the tailings, particularly the possibility of flow liquefaction. The coarse tailings from two of the KGHM mines (Rudna and Lubin) are used to raise the ring dam, and are deposited by spigotting on the beaches of the confining dams. The much finer tailings from the third mine (Polkowice) are deposited hydraulically directly into the pond. The range of particle size distribution of the coarser tailings was investigated by Lipinski (2000), and is shown in Fig. 39, together with the mineralogical composition and the range of specific gravity, G_s . The plasticity index of the fines from the tailings used to raise the dam does not exceed 10%.

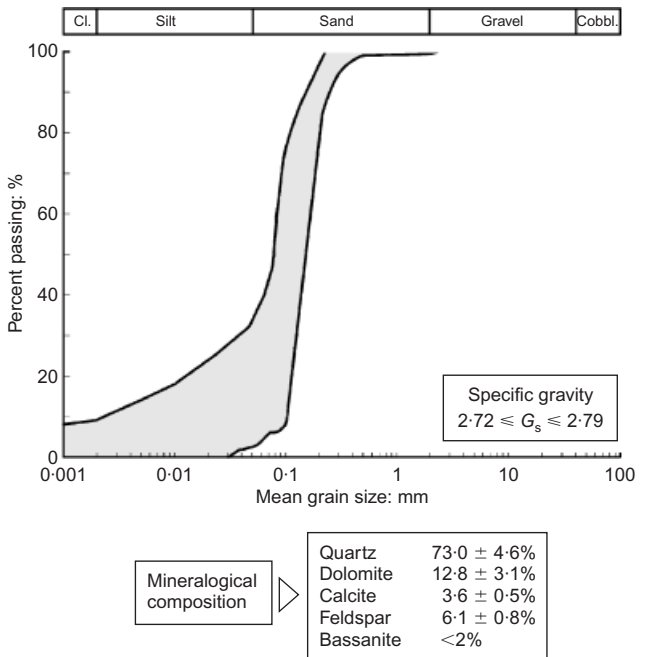


Fig. 39. Range of tailings grading (used to build the ring dam) and mineralogical composition

Because of the difficulties in sampling the tailings in their undisturbed state, their characterisation was carried out using a variety of in-situ tests, aimed at determining

- (a) spatial distribution of grading and index properties
- (b) depth of the saturation line below the beach and its changes as the dam is raised
- (c) undrained and drained shear strength, although the latter is not discussed here.

Hundreds of static cone penetration tests, both with (CPTU) and without pore pressure measurements (CPT), have been carried out. Examples of CPTU tests carried out on the beach of the East dam showing profiles of cone resistance (q_c) at various distances from the dam crest are shown in Fig. 40. This also illustrates that the value of q_c of the tailings generally decreases with the distance from the dam crest, a result of the increasing fines content (FC) as the test location approaches the pond. Similar conclusions can be drawn regarding the distribution of shear wave velocity, V_s , measured during seismic cone (S-CPTU) and seismic Marchetti (Marchetti *et al.*, 2008) dilatometer (S-DMT) penetration tests.

Overall, the down-hole geophysical methods, including the two types of seismic penetration test, have proved particularly useful for the characterisation of the tailings. In particular, the geophysical tests were of great help in assessing the risk flow failure of the tailings.

The measurement of compression wave velocity V_p in the CHTs enabled a simple and reliable distinction to be made between fully saturated and near-saturated tailings. This has become a standard approach, which, having been repeated periodically, enables the location and evolution of the saturation line in the tailings to be established.

Systematic measurements of V_s , when normalised with respect to the ambient effective stress (V_{s1}), are a useful index for coarse-grained soils at risk of liquefaction (Robertson *et al.*, 1992, 1995; Andrus & Stokoe, 2000; Olson, 2001; Liu & Mitchell, 2006; Idriss & Boulanger, 2008).

Measurements of V_p and V_s have been made periodically. Figs 41 and 42 present the results of CHTs carried out at the East and North dams, showing the position of the

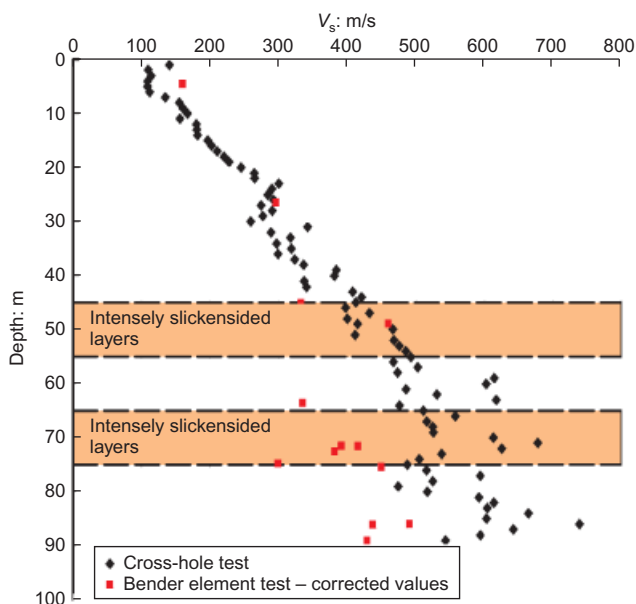


Fig. 38. East dam: shear waves velocity of Pliocene deposits

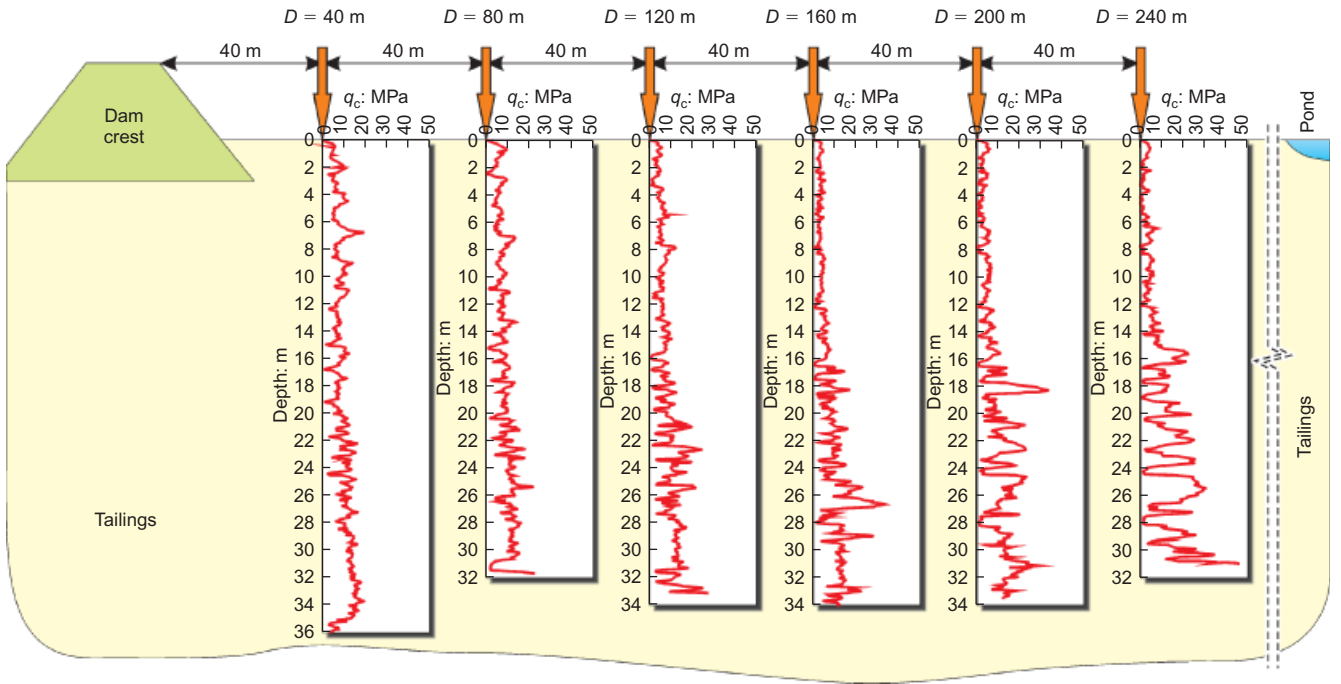


Fig. 40. East dam: example of static cone resistance profiles

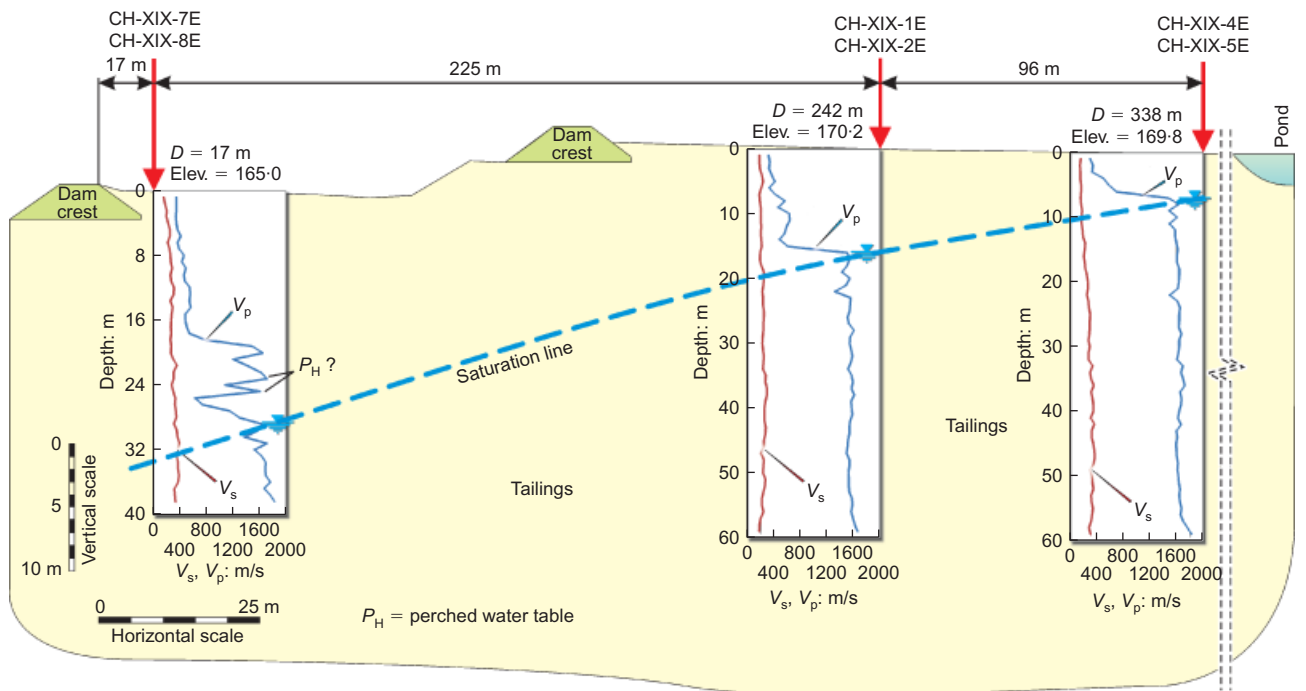


Fig. 41. East dam: location of saturation line from V_p measurements

saturation line. Since the compression wave velocity in water is ≈ 1450 m/s, V_p becomes a very accurate indication by which to recognise fully and near-saturated tailings, as seen in Fig. 43. For further details see Ishihara *et al.* (1998, 2004), Tsukamoto *et al.* (2002), Nakazawa *et al.* (2004) and Takahashi *et al.* (2006). It can be seen from Figs 41 and 42 that, thanks to the effectiveness of the internal drainage system in the depository, the position of the saturation surface in the tailings, particularly close to the dam crest, is well the below beach level. Table 6 summarises the monitoring results related to the saturation line for the period 1997–2011.

Figure 44 shows typical V_s profiles obtained from tests carried out below the beach of the East dam at a distance of

≈ 320 m from the initial dam crest at an elevation of 165 m asl (see also Fig. 41).

Together with the measured values of V_s , Fig. 44 also shows V_{s1} values normalised with respect to the current in-situ effective stresses, σ'_{v0} and σ'_{h0} . The values of V_{s1} below the saturation line, which is 6 m below the beach, are all greater than 160 m/s, the value which is approximately the borderline between contractive and dilative responses to shearing for tailings-like material during monotonic undrained triaxial tests (Robertson *et al.*, 1995). These relatively high values of V_{s1} indicate that the likelihood of a flow failure within the saturated tailings is low. Although not strictly pertinent to the issue of static liquefaction, Fig. 45 shows an example of the beneficial effects that even slightly

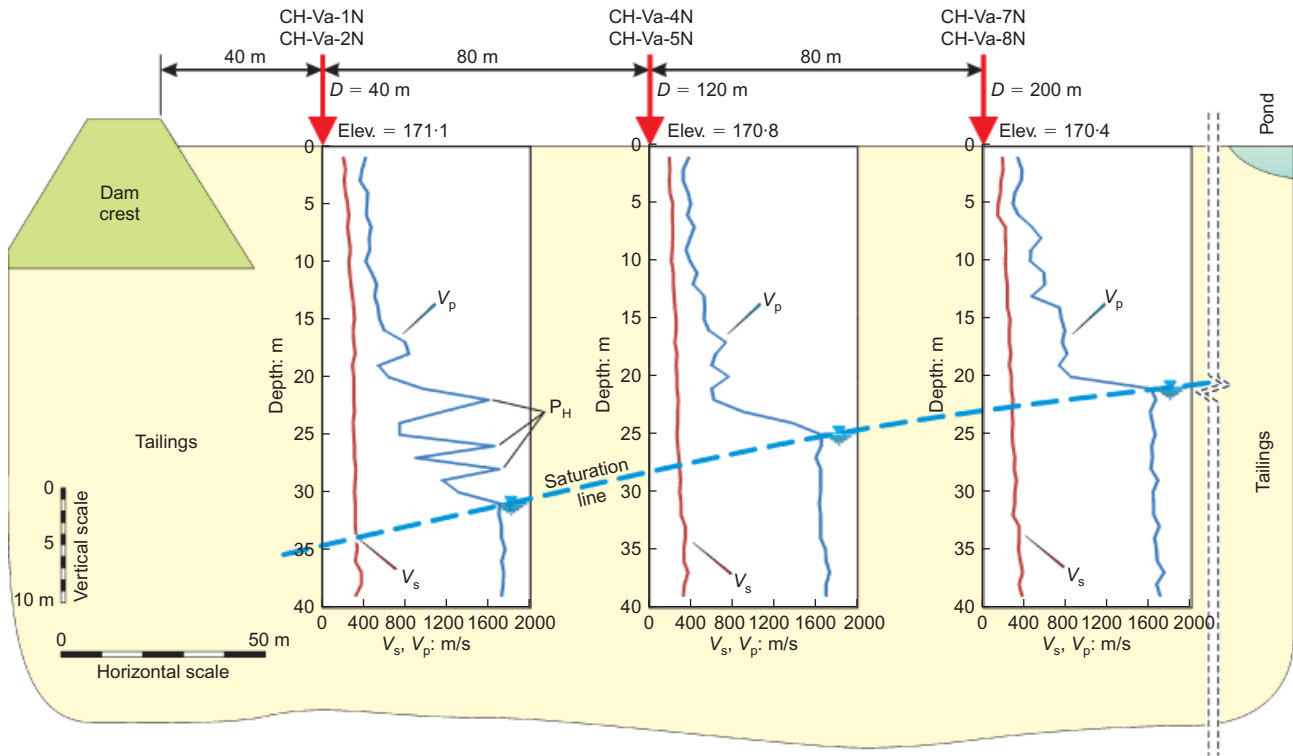


Fig. 42. North dam: location of saturation line from V_p measurements

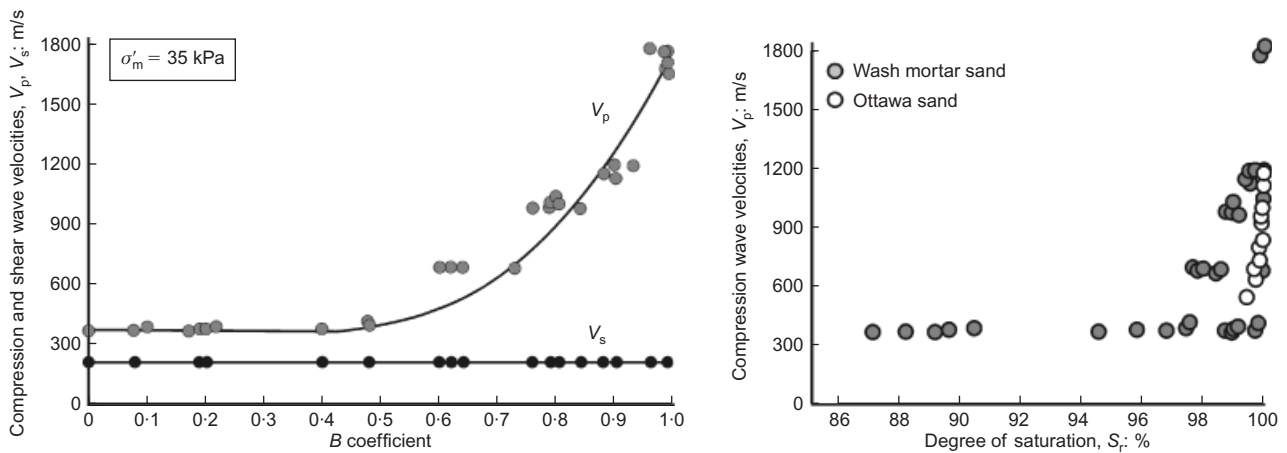


Fig. 43. Saturation degree plotted against compression waves velocity (Valle-Molina, 2006)

Table 6. Monitoring of saturation line location in tailings by V_p measurements (updated to October 2011)

Dam	Year	H_D : m	L_c/D_S : m	L_c/D_S : m	L_c/D_S : m
VIW	1993	22	NA	NA	152/12.0
VIIIW		24	NA	NA	155/10.5
VIIIW		31	40/14.0	120/10.5	200/7.5
XVIIIIE	2011	41	40/31.5	120/21.0	200/11.0
XIXE		62	17/37.0	242/16.0	338/8.0
VaN		38	40/31.0	120/25.0	200/21.0
VIIIW		50	41/31.0	132/25.0	217/21.0

Note: H_D = dam height; L_c = distance from the dam crest; D_S = saturation depth.

unsaturated states have on the resistance to cyclic liquefaction of Toyoura sand.

The classification and the index property tests shown in Table 7, the only other laboratory testing of the tailings has been undrained triaxial tests. Since 1998 (Dyvik (1998);

Dyvik & Høeg (1999); and Høeg *et al.* (2000)), ‘undisturbed’ sampling of the tailings has been carried out from hand-dug pits located in the beach, at varying distances from the dam crest. Thin-wall, sharp edged stainless steel samplers, 70 mm diameter and 140 mm height, were pushed into

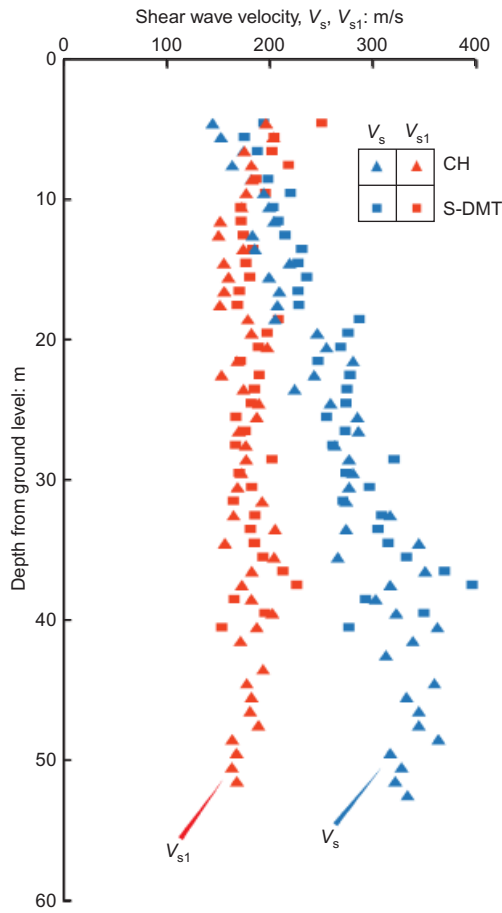


Fig. 44. East dam: shear waves velocity of tailings

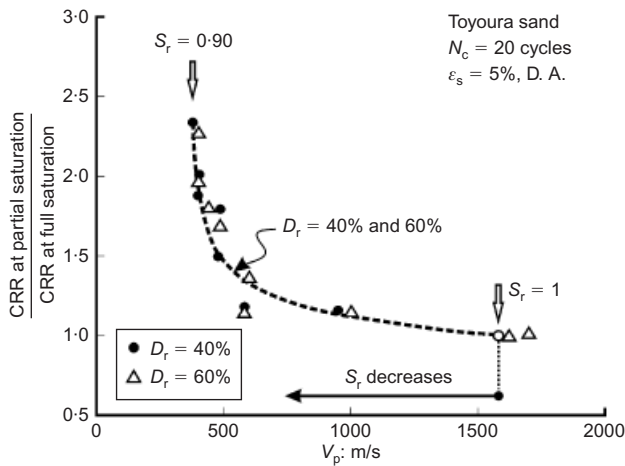


Fig. 45. Effect of partial saturation on the cyclic resistance ratio (CRR) of Toyoura sand (Ishihara *et al.*, 1998; Tsukamoto *et al.*, 2002); D. A., double cyclic shear strain amplitude

the base of the trial pits to take ‘undisturbed’ samples at depths 1 to 3 m below beach level. These samples were sent to three different geotechnical laboratories, where after saturation they were subjected to undrained triaxial tests. The ‘undisturbed’ samples were reconsolidated both isotropically (TX-CIU-C) and anisotropically (TX-CK₀U-C).

Although the sampling method adopted does not guarantee truly undisturbed specimens, the test results were very different from those obtained using reconstituted specimens (see Fig. 46).

Most ‘undisturbed’ specimens initially exhibited contractive behaviour, passed through the phase transformation (Ishihara, 1993) threshold, before showing continuous dilation. In contrast, all the reconstituted specimens, apart from a few prepared by slurry sedimentation, either exhibited flow collapse, or yielded at an undrained residual strength, S_{ur} (normalised with respect to σ'_{v0}) less than 0.2.

Moreover, as seen in Table 8 where the behaviour of undisturbed and reconstituted specimens is compared, not only is the strength of the ‘undisturbed’ samples greater, but the values of the small strain shear modulus G_0 are also consistently higher. Thus, it appears that the ‘undisturbed’ sampling procedure has at least partially preserved the in-situ fabric of the tailings. Encouraged by these positive results (from Lipinski, 2012), two further similar series of these tests were carried out (Lipinski, 2012), which yielded similar results for ‘undisturbed’ compared to ‘reconstituted’ specimens. The undrained shear strength S_u of the ‘undisturbed’ tailings obtained from the TX-CK₀U-C tests, normalised with respect to the axial consolidation stress σ'_a , is given in Fig. 47. Finally, Fig. 48 shows frequency histograms, subdivided depending on the value of consolidation stress σ'_a , for all the TX-CK₀U-C tests reported by Lipinski (2012). The results are classified according to the three possible modes of behaviour during undrained shear: dilative, contractive–dilative and contractive. This figure confirms that fully saturated Zelazny Most tailings are barely susceptible to flow failure, even under effective axial stresses as high as 1 MPa.

FUTURE DEVELOPMENT OF THE ZELAZNY MOST TAILINGS DISPOSAL FACILITY

As indicated in the section entitled ‘Behaviour of the ring dam’, the construction period for the Zelazny Most disposal facility, which commenced in 1977, is planned to continue until 2042. Thus construction is at present about half complete, with the need for additional storage capacity for $\approx 500 \times 10^6 \text{ m}^3$ of tailings in excess of the $518 \times 10^6 \text{ m}^3$ presently deposited. However, in light of the continuing horizontal displacements along the deep re-activated glacio-tectonic shear planes below the East and North dams, and the high construction pore pressures observed in the Pliocene clay, and because of the presence of other shear zones shown by the inclinometers, a review of the disposal development plans was considered to be mandatory.

Table 7. Index properties of Zelazny Most tailings

$32^\circ \leq \phi'_{cv} \leq 34^\circ$			$26.9 \leq G_s \leq 27.2$		
L_c : m	FC: * %	e_0	e_{max}	e_{min}	D_r : %
40	14.5 ± 4.9	0.798 ± 0.055	1.023 ± 0.028	0.531 ± 0.028	46.4 ± 8.2
100	18.9 ± 7.5	0.797 ± 0.032	1.034 ± 0.037	0.513 ± 0.036	45.6 ± 8.2
140	24.7 ± 11.2	0.847 ± 0.032	1.076 ± NA	0.510 ± NA	36.3 ± 5.8
200	24.8 ± 6.3	0.897 ± 0.077	1.076 ± 0.049	0.513 ± 0.034	29.3 ± 7.5

* Fine content, low-plasticity silts.

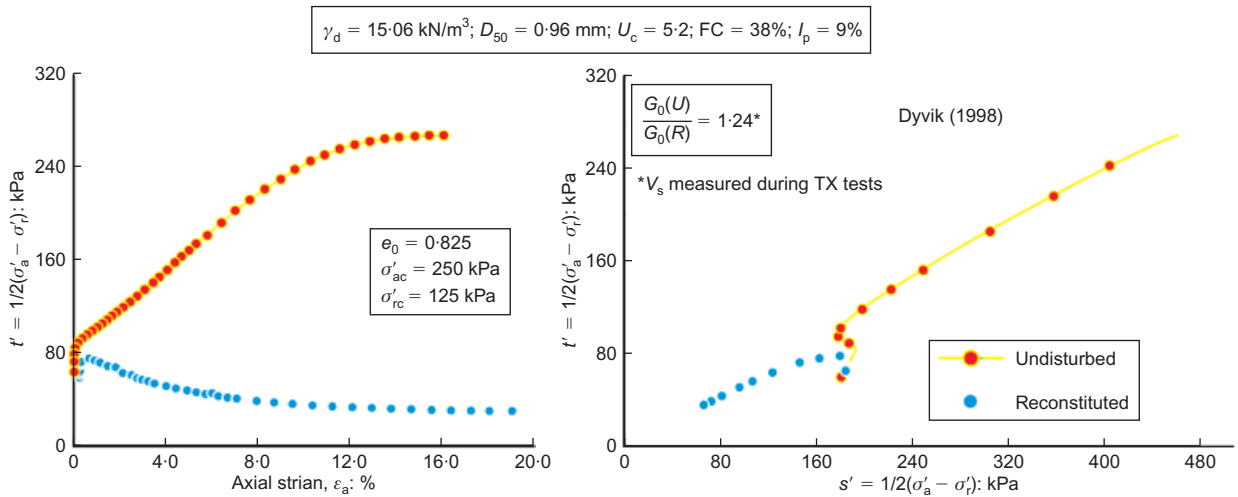


Fig. 46. Undrained triaxial compression tests on specimen consolidated in K_0 -condition (TX-CK₀-C tests) on undisturbed and reconstituted tailings specimens (Dyvik, 1998)

Table 8. Undrained triaxial tests results on saturated tailings (Dyvik, 1998)

L_c : m	FC: %	e_0	Test* type	B range	$(G_0)_1$: bar	$(G_0)_1 U / (G_0)_1 R$
40	22	0.811	U	0.968–0.991	849	1.23
		0.809	R	0.976–0.996	691	
120	24	0.806	U	0.950–0.987	851	1.20
		0.821	R	0.971–0.994	709	
200	28	0.810	U	0.967–0.995	857	1.27
		0.808	R	0.980–0.995	674	

* TX-CAU-C, σ'_{ac} : 50, 250 and 500 kPa; $\sigma'_{rc}/\sigma'_{ac}$: 0.5; $(G_0)_1 = G_0$ at $\sigma'_m = 1$ bar; FC: fines content, low-plasticity silt; U: undisturbed specimens; R: reconstituted specimens.

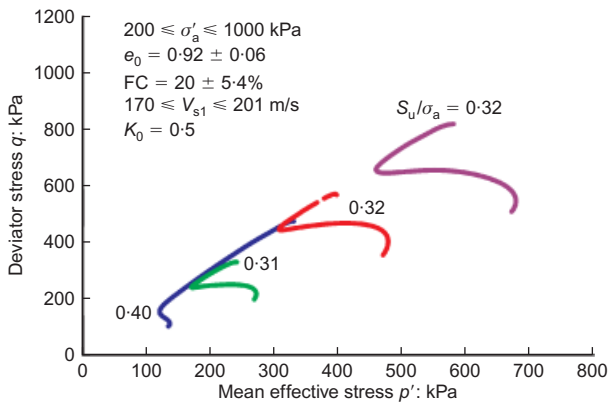


Fig. 47. Undrained strength of undisturbed tailings (adapted after Lipinski (2012))

Because of the large horizontal displacement experienced by the North dam, the first important decision was to adopt a 3–5-year idle period, during which the dams will not be raised above elevation 180 m asl. This idle period, which is scheduled to start in 2017, will allow a partial dissipation of the excess pore pressures in the foundation below the ring dam, and will provide time to observe the effectiveness of the stabilisation measures being adopted for the North dam. Meanwhile, to allow tailings deposition to continue during the idle period, a new storage facility, the ‘southern extension’ will be built. This is to be located adjacent to the South dam, and will have a capacity of $\approx 115 \times 10^6 \text{ m}^3$ (see Fig. 49).

Furthermore, the idle period will allow time to examine the feasibility of plans for the future development of the Zelazny Most facility. This future development requires the ring dam to be raised to 195 m asl, and to store the tailings as paste, in cones up to an elevation of 212 m asl.

Given the considerable geotechnical problems at Zelazny Most, the future development is a significant challenge for the engineers responsible for the stability of the dams. Of paramount importance is to explore the stability of the ring dam foundation. Until 2010 this was evaluated solely by means of the limit equilibrium method. In that year KGHM commissioned the NGI to carry out a series of FEAs to explore the stability of the East dam. This was done by modelling the soil behaviour through constitutive laws of increasing complexity.

As described in various NGI reports (NGI, 2010, 2011, 2013a, 2013b), in addition to static FEAs, a dynamic analysis was also carried out to explore the effects of mining-induced seismicity on the stability of the East dam and of the tailings. This analysis of mining seismicity is not covered here as it has limited impact on the stability of the ring dam, and only a minor influence on the susceptibility of tailings to flow failure.

The results of the NGI static analyses, summarised in the following section, take into account the observed excess pore pressures, the stabilisation measures that have already been implemented and the active glacio-tectonic shearing planes encountered in cross-section XVIIE.

- (a) The analyses, particularly when using the more advanced constitutive models of soil behaviour, yield computed horizontal surface displacements, measured at the starter

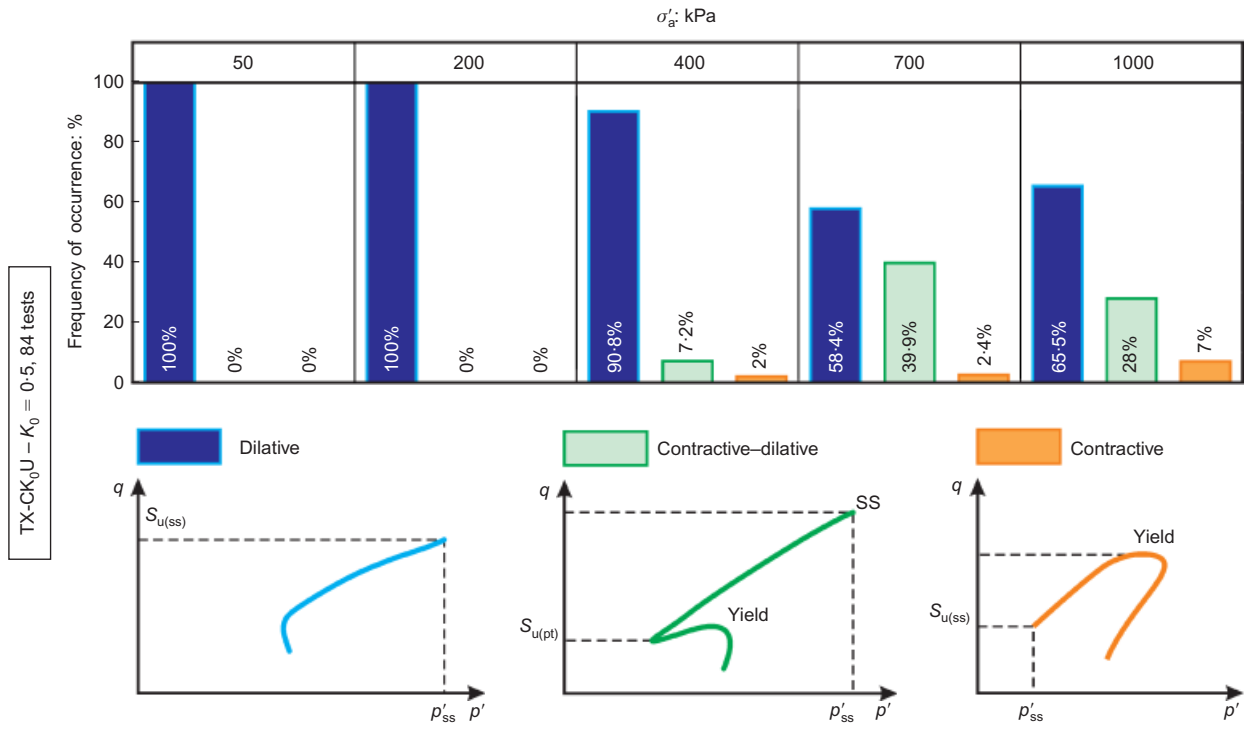


Fig. 48. Histogram of the undrained triaxial tests results (adapted after Lipinski (2012))

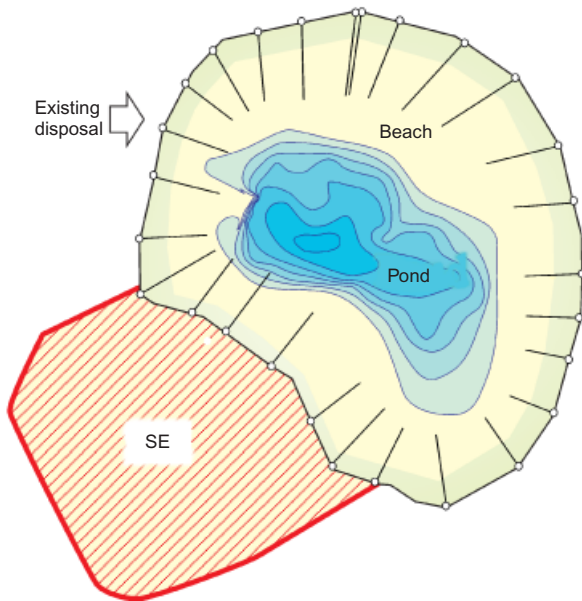


Fig. 49. Southern extension

dam crest (BM-208, Fig. 50 (note that this figure also shows the results of the back analysis carried out by SGI and discussed next)), that are in very good agreement with the geodetic survey.

- (b) At a dam elevation of 175 m asl the factor of safety $F_S = 1.45$, inferred from the FEAs using an elastic-perfectly plastic soil model, is in good agreement with the value $F_S = 1.40$ computed by the limit equilibrium method.
- (c) By raising the dam in steps of 1.0–1.5 m the FEAs predict failure of the dam when the dam crest elevation reaches between 190 m and 198 m asl, depending on the constitutive soil model and the soil parameters that are used. In all the cases that have been considered, failure

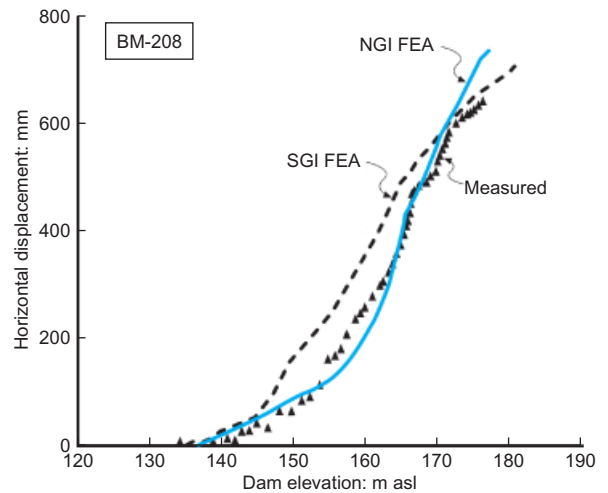
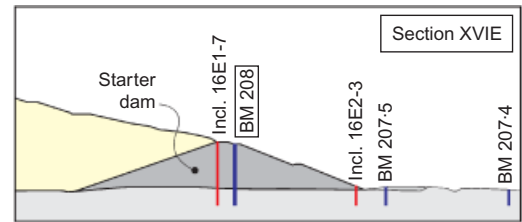


Fig. 50. Cross-section XVIIE, FEA: computed plotted against measured surface horizontal displacements

shows as a pronounced increase of the horizontal displacement rate.

- (d) These analyses suggest that a form of ultimate limit damage state in terms of the total horizontal displacement and of displacement rate, expressed as a function of the dam crest elevation, might be used.
- (e) The FEAs suggest that it is unlikely to be feasible to raise the crest of the East dam to the planned elevation of

195 m asl without relying on both the beneficial effects of a significant reduction of the excess pore pressure during the idle period, and also on the effectiveness of stabilisation measures similar to those at the East dam. Neither of these beneficial effects can be taken for granted given the geological complexities, but must be confirmed through continuous monitoring. To ensure the continuity of tailings disposal over the next 30 years many alternative solutions are being examined, including the re-activation of the decommissioned tailings disposal Gilow, dry stacking of tailings to reduce significantly their volume, and increasing the storage capacity of the southern extension.

If the 2017 idle period and the various stabilisation measures are not effective in allowing the ring dam to be raised to an elevation of 195 m asl, there is another alternative. This would be to install large-diameter, deep, structural shafts just downstream of the dam toe (see Fig. 51).

Preliminary FEAs of this proposal carried out by NGI (2013a, 2013b) have explored the effect of cylindrical shafts of 18 m diameter and with wall thickness of 1.9 m, with depths from 115 to 135 m, spaced 50 m apart; this is feasible thanks to the new generation of hydromills capable of constructing diaphragm wall panels to a depth in excess of 200 m.

As with the previous analyses without a shaft, the results suggest that the stability of the dam is controlled by the magnitude of the allowable horizontal displacement. Based on the NGI analyses, the effectiveness of the shafts appears quite limited. Assuming a horizontal displacement of the starter dam of 1.5 m to be the threshold for the ultimate damage state, such a value is attained at about dam elevation 205 m asl.

However, because this value results from analyses that involve both simplified constitutive relationships and the use of a conservative peak ϕ' value ($= 14.5^\circ$) for the bulk Pliocene clay, the analyses underestimate the shaft efficiency. To add further detail on the use of deep shafts as a potential stabilisation measure for the North dam, an FEA carried out independently by Studio Geotecnico Italiano (SGI) of cross-section XVIIE is described (Rocchi & Da Prat, 2014). Before going into details it is worth pointing out that results of the analyses by both NGI and SGI are comparable because they

consider the same foundation soil profile, dam geometry and construction rate.

The SGI analyses assumed effective stress coupled consolidation, and investigated the dam behaviour without a shaft in two dimensions, and with shafts in three-dimensional conditions. The FEA model with the shaft included is shown in Fig. 52.

Displacement along the bottom boundary is prevented, while rollers are applied at the vertical boundaries. The finite-element mesh consists of 61 272, 15-noded tetrahedral zone elements with 171 009 nodes.

The characteristics of the shaft adopted in the model are shown in Fig. 52, where D_0 is the external diameter, t the wall thickness, L the length and s the spacing between shafts. The shaft was modelled by cylindrical shell elements, and interface elements were employed to avoid refining the mesh around the shaft. The constitutive model adopted for the shell elements and related material properties are representative of good quality concrete. The constitutive model adopted for the Pliocene clay was developed by Rocchi *et al.* (2012) for mechanically overconsolidated, high-plasticity clay, taking into account strain softening in shearing.

Strain softening is a result of one or more of the following phenomena: loss of dilatancy/interlocking, previous

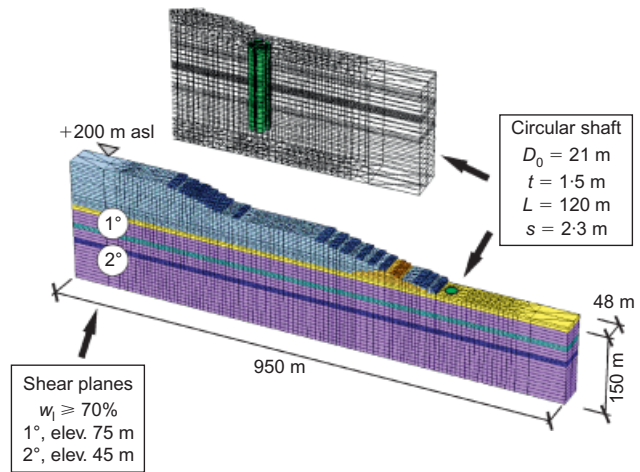


Fig. 52. East dam: finite-element model with circular shaft

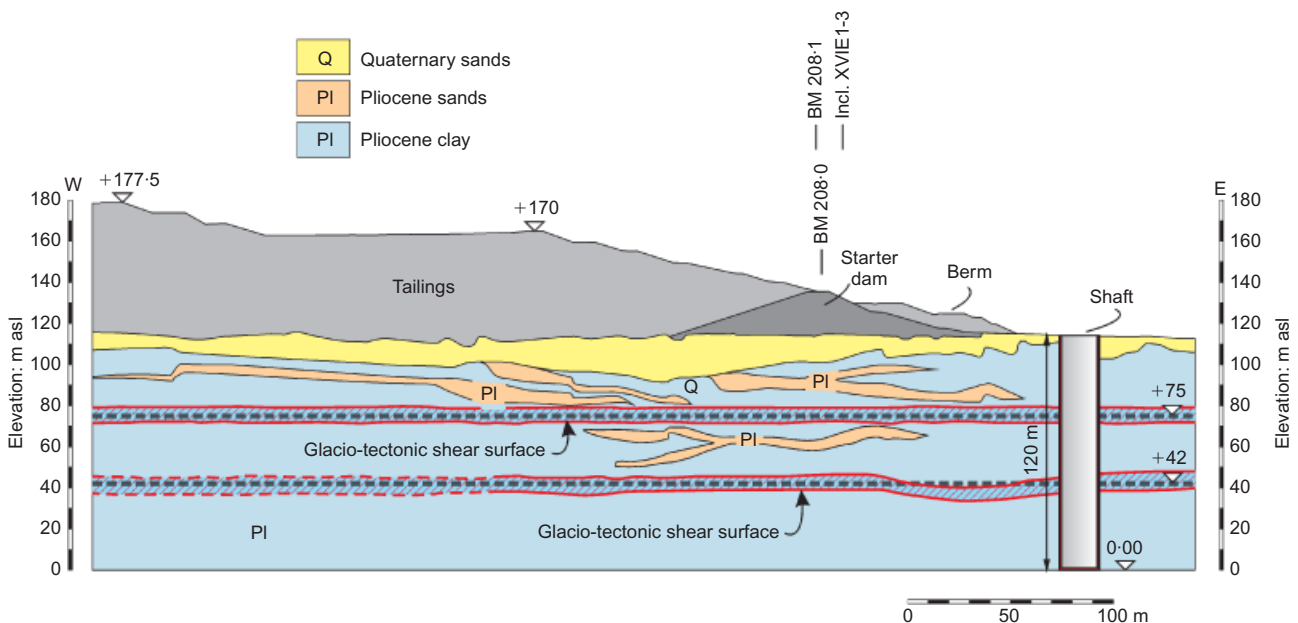


Fig. 51. East dam: cross-section XVIIE with shaft

consolidation under a very high overburden stress and the development of preferred orientation of the platy clay particles on the slip plane along the direction of shearing.

The constitutive model adopted accounts for both volumetric and kinematic hardening, allowing the elasto-plastic strains to be controlled by the kinematic hardening yield surface bubble, located inside the modified Cam Clay limit state boundary surface (see Al-Tabbaa & Muir Wood, 1989; Atkinson & Stallebrass, 1991; Stallebrass & Taylor, 1997).

The strength softening mechanism, owing to the platy clay particles' orientation, was modelled with ϕ'_{cv} degradation, regarded as a function of the cumulative deviatoric plastic strain invariant (ϵ_d^p) (Potts *et al.*, 1990, 1997; Kovacevic *et al.*, 2004, 2013). The functions ϕ'_m plotted against ϵ_d^p adopted in the analyses for both the bulk Pliocene clay and the two active glacio-tectonic shear planes are shown in Fig. 53.

The coefficient of permeability k was assumed to vary with the current specific volume ($1 + e$), in line with recommendations by Taylor (1948) and Tavenas *et al.* (1983). The behaviour of the Quaternary sands was modelled assuming a simple non-associated elasto-plastic constitutive model, by way of the Mohr–Coulomb failure criterion, according to Vermeer & De Borst (1984).

Following the conclusion reached in the ‘Tailings’ section that the risk of flow failure of the tailings is low, and given that the stability of the ring dam is controlled by the foundation soils rather than by the tailings, in the analyses the behaviour of the tailings was modelled adopting the same constitutive law as for the Quaternary sands.

The FEAs for the dam with a shaft were performed in the following stages.

- (a) Imposition on the Pliocene clay of an overburden stress of 10 MPa, exerted on the ground surface by the ice sheet. In this phase, two simplifying assumptions were introduced: a single glacial cycle was modelled, and the Pliocene clay was taken to be in a truly normally consolidated state, with I_v and σ'_{v0} lying on the Burland's (Burland, 1990) ICL_{oed} line. The shear strength of the clay linked to this assumed initial state corresponds to $\phi'_m = \phi'_{cv}$ and $c' = 0$. The possibility of some shear degradation of ϕ'_{cv} is ignored.
- (b) Melting of the ice sheet, that is, removal in drained conditions of the vertical load due to the ice, resulted in a stress path that follows the swelling line of the mechanically overconsolidated material, leading to the current state in terms of I_v and σ'_{v0} being located well below the intrinsic compression line, ICL_{oed}. At this point in the analysis the in-situ stress state exhibited an increase of K

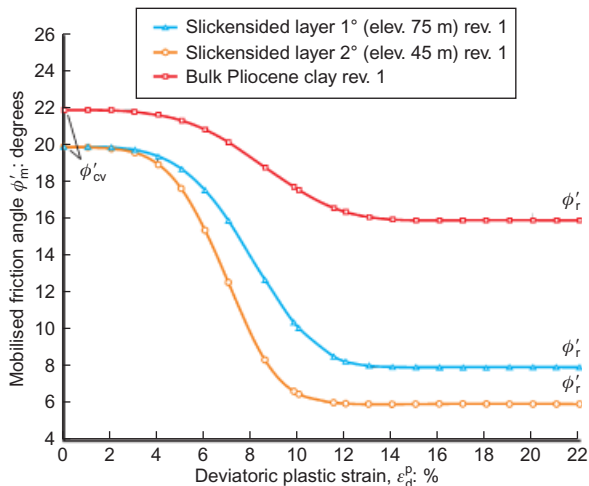


Fig. 53. East dam: 3D FEA, shear strength degradation functions

($= \sigma'_{h0}/\sigma'_{v0}$), which, at the end of ice melting, approached conditions close to passive failure (see Fig. 29). During swelling the plastic strain (ϵ_d^p), Fig. 53, promotes both dilation and alignment of the platy clay particles in the direction of shearing, with a consequent progressive reduction of the available mobilised value of ϕ'_m . This phenomenon is particularly marked within the intensely slickensided high-plasticity clay horizons, as can be seen from Fig. 54. This figure shows that on these horizons, $\phi'_{cv} = 20^\circ$ has decayed to values of 9.5° and 10.0° in the intensely slickensided layers 1 and 2 respectively by the end of ice melting. What emerges from Fig. 54 corroborates the results reported by Chandler (2010) regarding the important changes occurring in overconsolidated sedimentary clays when subjected to significant unloading/erosion.

- (c) The dam construction was simulated up to crest elevation 180 m asl, including the crest relocation towards the pond and the construction of the stabilising berm.
- (d) Push-over analyses raising the dam above 180 m asl to reach the ‘failure condition’ showed a rapid increase in the horizontal displacement as the dam crest elevation increased.

Figure 55 shows the pattern of horizontal displacement within the dam body with the crest at 195 m asl; at this point the maximum horizontal displacement equals 1.3 m. The corresponding distribution of horizontal displacement with depth computed for three different dam elevations at the location of BM-208 is shown in Fig. 56. These analyses are in good agreement with those carried out by NGI, and confirmed that the further rise of the dam height above an elevation of 180 m asl does not offer an adequate margin of safety unless accompanied by appropriate stabilisation measures.

Assuming that the stabilisation measures now under construction at the North dam yield positive results, and assum-

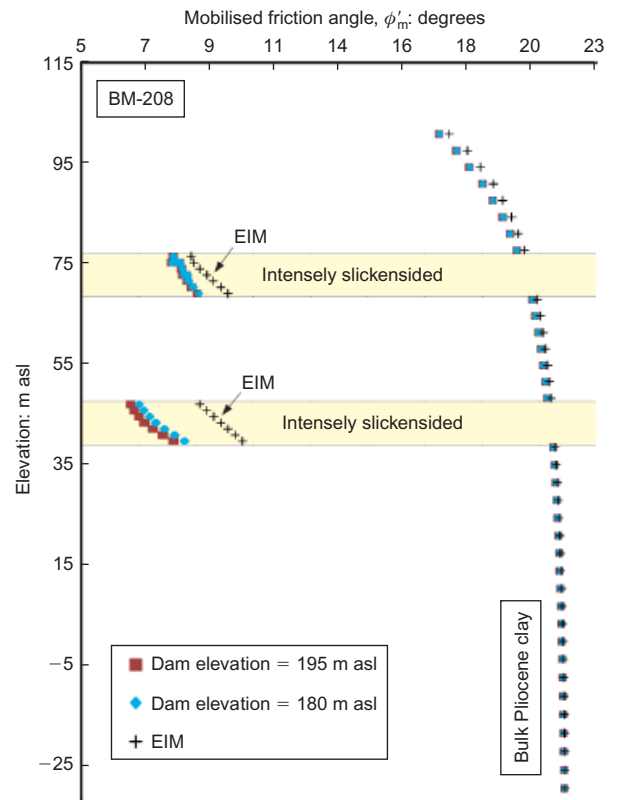


Fig. 54. Cross-section XVIIE: 3D FEA model, computed ϕ'_m degradation

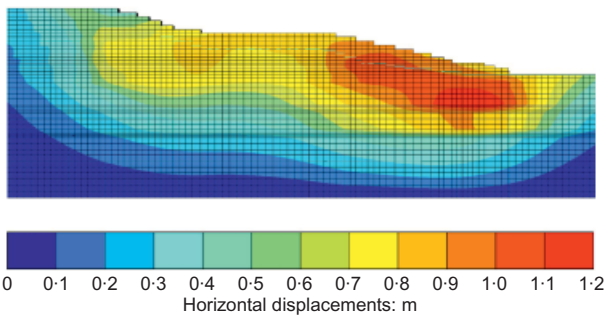


Fig. 55. Cross-section XVIIE: 3D FEA model, pattern of horizontal displacements, dam at elevation 195 m asl

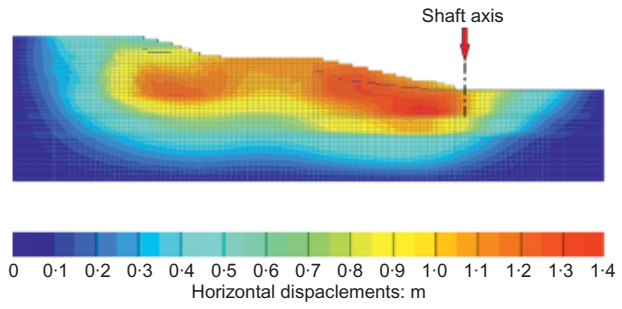


Fig. 57. Cross-section XVIIE: 3D FEA model, pattern of horizontal displacements with shaft, dam at elevation 210 m asl

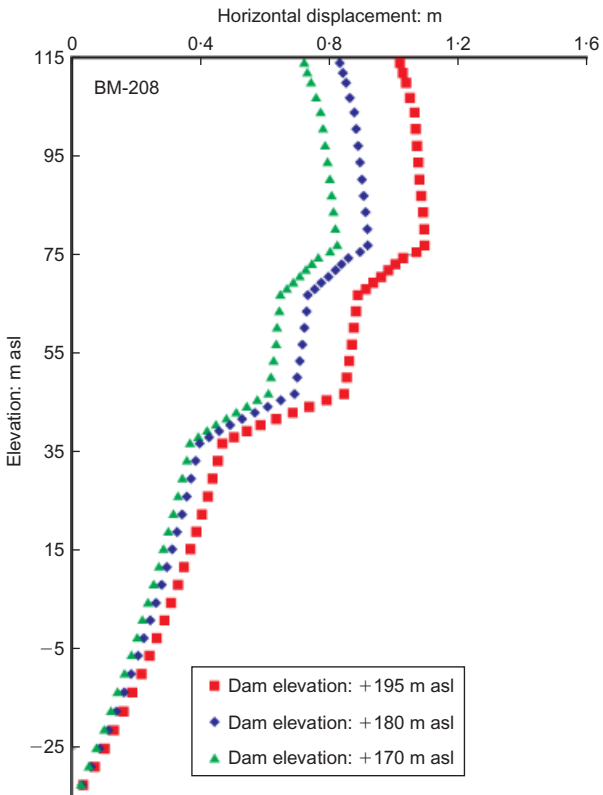


Fig. 56. Cross-section XVIIE: 3D FEA model, without shaft, computed total horizontal displacement profiles

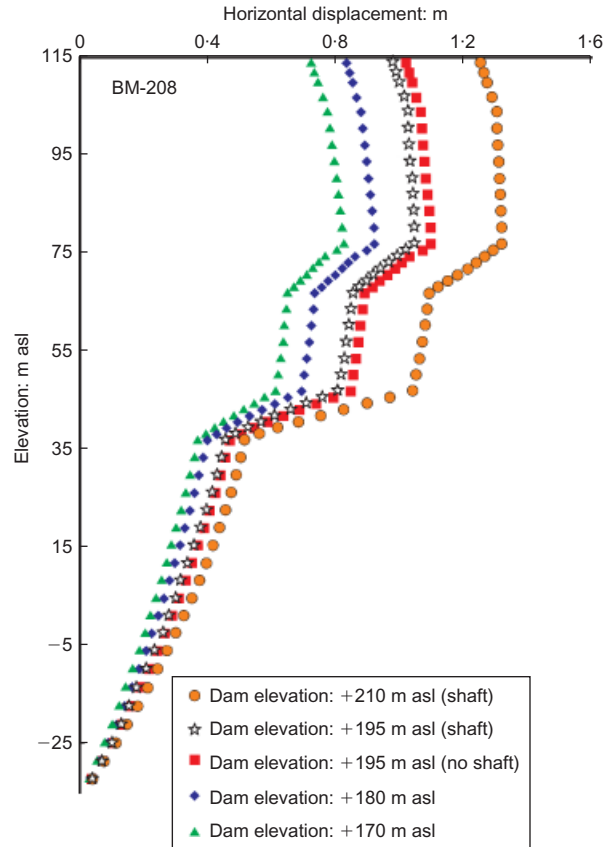


Fig. 58. Cross-section XVIIE: 3D FEA model, computed total displacements profiles

ing beneficial results from the idle period, it is intended to continue to raise the ring dam (including the remedial measures implemented at the East dam), with rigorous use of the observational method. However, if the results of monitoring do not allow safe construction, a possible alternative solution is the use of deep structural shafts, as shown in Fig. 51.

The feasibility and effectiveness of this possible remedial solution has also been examined using FEAs. Vertical shafts 120 m deep, with the properties shown in Fig. 52, were ‘wished-in-place’ in the analysis, and the dam was raised up to an elevation of 210 m asl at the same construction rate as previously.

Figure 57 shows the corresponding pattern of horizontal displacements within the dam body, with the shafts in place, while Fig. 58 shows the horizontal displacement profiles with depth computed for the location of BM-2008 for various dam crest elevations.

Both Figs 57 and 58 indicate that the dam, with the shaft in place, when raised to 210 m asl exhibits a maximum horizontal displacement of ≈ 1.4 m. To examine further the performance of the dam with the shafts in place, horizontal

displacement profiles were computed for points A and B from the start of construction, as shown in Fig. 59. Point A is located 2 m downstream of the shaft axis, while point B is midway between two adjacent shafts. The profiles show the total horizontal displacement for dam elevations 195 m, 200 m, 208 m and 210 m asl.

At a dam elevation of 210 m asl the maximum horizontal displacement of point A is 1.1 m, which occurs at ground level, while at point B the maximum displacement is 1.2 m, at elevation 75 m asl at slickensided horizon 1 (see Fig. 52). As shown in Figs. 57–59, the dam approaches ‘failure’ in terms of excessive horizontal displacement at elevation 210 m asl; this is confirmed by the lack of numerical convergence in the computation when attempting to raise the dam height by an additional 1.5 m. Moreover, to understand better the role played by the shaft in controlling the movements of the dam, it is necessary to compare the displacement profiles of Fig. 59 with those of Fig. 60, which show the displacements at point A after shaft installation. There is

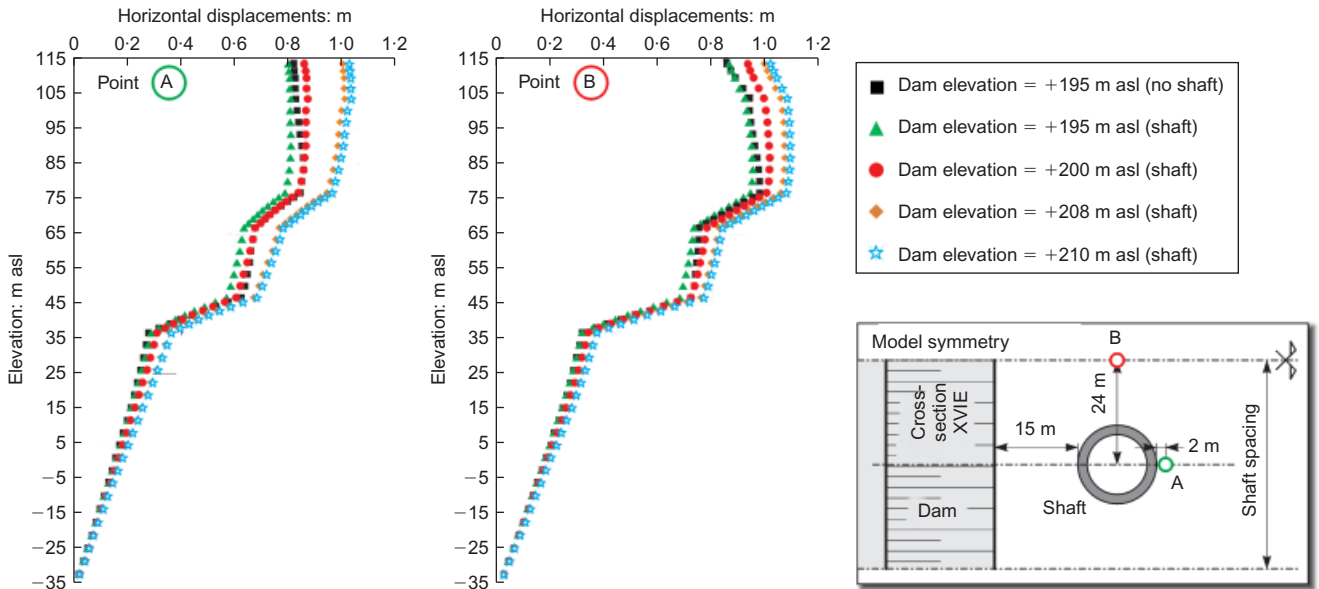


Fig. 59. Cross-section XVIIE: 3D FEA model, total horizontal displacements profiles at points A and B since start of dam construction

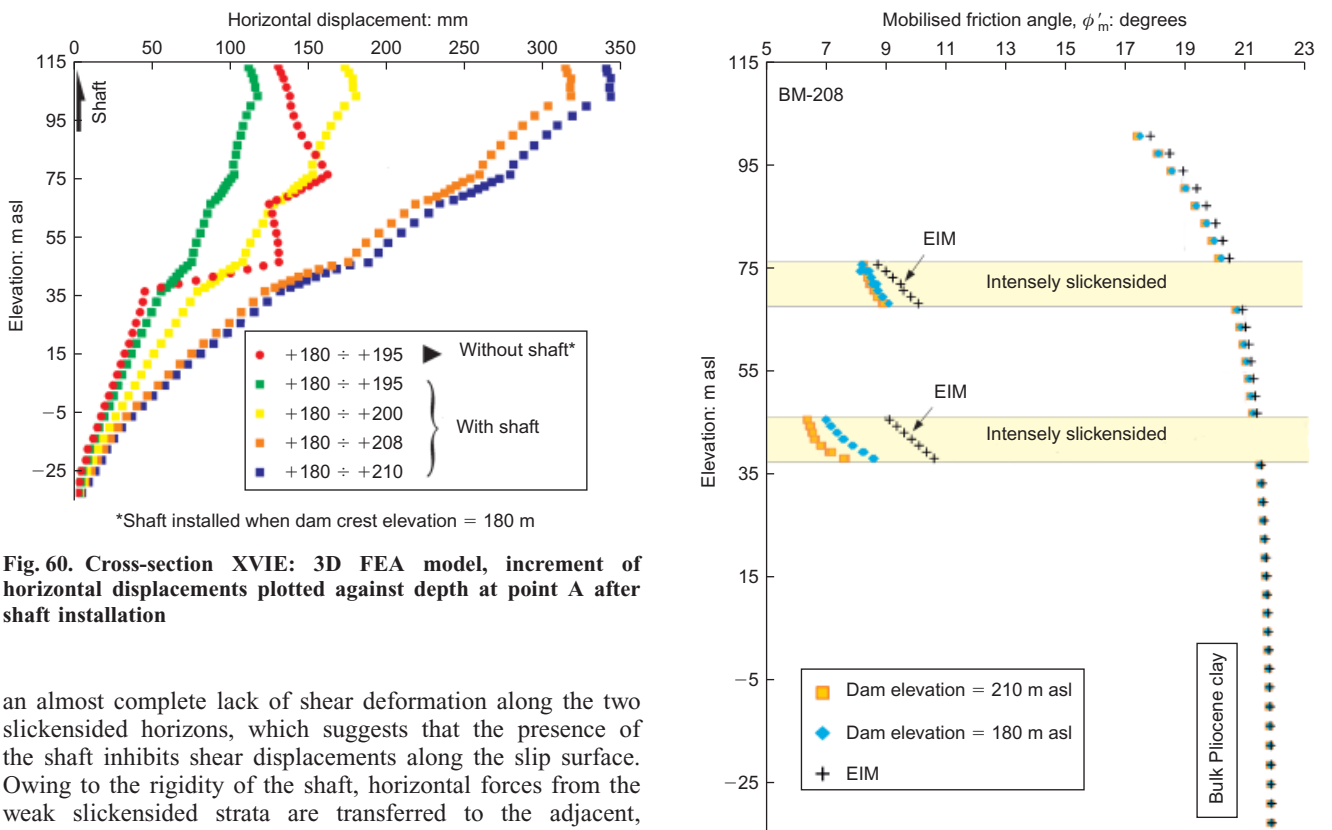


Fig. 60. Cross-section XVIIE: 3D FEA model, increment of horizontal displacements plotted against depth at point A after shaft installation

an almost complete lack of shear deformation along the two slickensided horizons, which suggests that the presence of the shaft inhibits shear displacements along the slip surface. Owing to the rigidity of the shaft, horizontal forces from the weak slickensided strata are transferred to the adjacent, much stronger, bulk Pliocene clay, which acts as a prop. Similar situations have been described by Alencar *et al.* (1994) and Wedage *et al.* (1998) in comparable, although simpler, geotechnical conditions.

Figure 60 also shows the computed profile of horizontal displacements when raising the dam from elevation 180 m asl to elevation 195 m asl, in the absence of shaft, which shows significant displacement along the two active shearing planes. This figure also suggests that the large increase of the surface horizontal displacements when the dam is raised from elevation 200 m asl to elevation 208 m asl can be attributed mainly to the rigid-body rotation of the shaft. As shown in Fig. 61, even in the presence of shaft, particularly in the deeper slickensided horizon 2, there is further degradation of ϕ'_m , which approaches the value close to ϕ'_r .

Fig. 61. Cross-section XVIIE: 3D FEA model: computed ϕ'_m degradation

In contrast, the values of ϕ'_m of the bulk Pliocene clay with the dam crest at elevation 210 m asl show that after ice melting the bulk clay did not suffer from any appreciable strength degradation.

The writer is fully aware that the shaft analysis presented here is a very preliminary attempt to explore the feasibility of the use of deep shafts as a possible stabilisation measure. Owing to its cost, this is an extreme solution by which to raise the dam to an elevation of 195 m asl (and to store the tailings paste to elevation of 212 m asl). However, con-

sidering the significant challenge of enabling completion of the Zelazny Most facility, deep shafts need to be considered as a remedial measure in case more conventional stabilisation measures prove to be inadequate in such a complex geological and geotechnical environment.

CLOSING REMARKS

- (a) The Zelazny Most area is affected by a number of geotechnical hazards and the flow liquefaction of the stored tailings, thus the stability of the confining dams is certainly the most relevant.
- (b) The most important geotechnical hazard to the stability of the dams is a consequence of their location in an area that, during the Pleistocene, experienced at least three major glaciations. The ice sheets, over 1000 m thick, that overrode the area induced substantial glacio-tectonic phenomena; the most important from a geotechnical point of view is the formation of extensive sub-planar shear encountered in slickensided high-plasticity clay horizons, which controls the stability of the ring dam.
- (c) Overall, as a result of the glacio-tectonic disturbance, the Pliocene deposits exhibit an extremely pronounced spatial variability, making the formulation of realistic geological and geotechnical models impracticable. This has triggered the KGHM decision to develop the Zelazny Most depository, applied during the overall 70 years of its planned operation according to the observational method (Peck, 1969, 1980).
- (d) At present, the Zelazny Most project is half-way through its planned operation time. The ring dam elevation is close to 180 m asl. Considering the horizontal displacements exhibited by the East and North dams, the high construction pore excess pressure measured in the foundation clay and the results of NGI's FEAs, the mine following IBE advice, has accepted 3–5 years of idle period, during which the raising of the ring dam will be suspended. In order to avoid the interruption of the mining operation, an auxiliary southern depository with a storage capacity of $\cong 115 \times 10^6 \text{ m}^3$ has been designed and its construction is close to being started.
- (e) As to the flow liquefaction hazard, its likelihood has been attenuated by evidences that
- the depth to phreatic surface in the tailings, especially in the vicinity of the dam shell, is found at relevant depths below the beach level
 - the majority of undisturbed specimens of fully saturated tailings, during undrained monotonic triaxial tests, exhibit contractive–dilatant and dilatant type of behaviour.
- (f) The future of the Zelazny Most ring dam, which in 2042 will reach the elevation of 195 m asl, with the tailings paste stored on the beaches up to elevation of 212 m asl, will require
- continuous enhanced monitoring, within the framework of the continued strict application of the observational method
 - consideration of the complex geology, the need to conceive and be ready to implement measures capable of mitigating the horizontal dam displacements; this will involve considering the already-known active shear planes, as well as those dormant existing in the foundation clay, which may be reactivated after the resumption of the ring dam raising.

ACKNOWLEDGEMENTS

The author's work was made possible by the support and assistance of a number of people to whom he would like to

express his sincere thanks. First, the author is grateful to the mine (KGHM), for making available the Zelazny Most information and data. Gratitude and recognition are also owed to IBE and Polish geotechnical expert colleagues, whose expertise, and many discussions and good teamwork, have been crucial during over 20 years of joint efforts on this demanding project. Special thanks and recognition in particular are extended to Professor R. Chandler for his inspiration and continuous back-up. His advice has enriched the author from both a professional and a critical point of view. Of the consultants assisting IBE, special appreciation is owed to NGI for overseeing the monitoring instrumentation and for carrying out many high-quality deformation and stability finite-element analyses. Finally, the author wishes to credit the people of Studio Geotecnico Italiano for their assistance with the research, first and foremost Engr G. F. Rocchi.

NOTATION

A_s	Skempton's pore pressure coefficient
A_c	clay activity
B	Skempton's pore pressure coefficient
c'	effective stress cohesion intercept
D	distance in metres from the dam crest
D_r	relative density
D_s	saturation depth
D_0	shaft diameter
D_{50}	mean grain size
e_{\max}	maximum void ratio
e_{\min}	minimum void ratio
e_0	initial void ratio
F_s	factor of safety
G_0	small strain shear modulus
G_{01}	small strain shear modulus at σ'_a of 98.1 kPa
G_s	specific gravity
H_D	dam height
I_L	liquidity index
I_p	plasticity index
I_v	void index
K	coefficient of horizontal stress
K_0	coefficient of earth pressure at rest
k	coefficient of permeability
L	shaft length
L_c	distance from the dam crest
M_c	q/p' at failure in compression tests
M_e	q/p' at failure in extension tests
N_c	number of stress cycles
P_H	perched water table
p'	mean effective stress
p_k	suction measured on undisturbed sample
p_{ss}	mean effective stress at steady state
q	deviator stress
q_c	cone resistance
S_r	degree of saturation
S_u	undrained shear strength
$S_{u(pt)}$	undrained shear strength at phase transformation
$S_{u(ss)}$	undrained shear strength at steady state
s	shaft spacing
$s_{h \max}$	maximum horizontal displacement at shear plane elevation
s_{h0}	inclinometer head horizontal displacement
t	shaft wall thickness
U_c	uniformity coefficient
V_p	compression wave velocity
V_s	shear wave velocity
V_{s1}	normalised shear wave velocity
w_l	liquid limit
w_n	natural water content
w_p	plastic limit
γ_d	dry unit weight
γ_t	bulk unit weight
ε_a	axial strain
ε_d^p	deviatoric plastic strain
ε_r	radial strain
ε_s	shear strain

σ'_a	axial effective stress
σ'_{ac}	axial consolidation stress
σ'_h	horizontal effective stress
σ'_{h0}	horizontal geostatic effective stress
σ'_r	radial effective stress
σ'_{rc}	radial consolidation stress
σ'_v	vertical effective stress
σ'_{v0}	vertical geostatic effective stress
$\sigma'_{v\max}$	maximum past effective overburden stress
ϕ'	peak friction angle
ϕ'_c	friction angle from triaxial compression tests
ϕ'_{cv}	friction angle at critical state
ϕ'_e	friction angle from triaxial extension tests
ϕ'_m	mobilised friction angle
ϕ'_r	residual friction angle

REFERENCES

- Al-Tabbaa, A. & Muir Wood, D. (1989). An experimentally based 'bubble' model for clay. In *Proceedings of the 3rd 'Numog', numerical models in geomechanics, Niagara Falls, Canada* (eds S. Pietruszczak and G. N. Pande), pp. 91–98. New York, NY, USA: Elsevier.
- Alencar, J., Morgenstern, N. R. & Chan, D. H. (1994). Analysis of foundation deformations beneath the Syncrude tailings dyke. *Can. Geotech. J.* **31**, No. 6, 868–884.
- Anantanasakul, P., Yamamuro, J. A. & Lade, P. V. (2012). Three-dimensional drained behaviour of normally consolidated anisotropic kaolin clay. *Soils Found.* **52**, No. 1, 146–159.
- Andrus, R. D. & Stokoe, K. H. (2000). Liquefaction resistance of soils from shear-wave velocity. *J. Geotech. Geoenviron. Engng, ASCE* **126**, No. 11, 1015–1025.
- Atkinson, J. H. & Stallebrass, S. E. (1991). A model for recent history and non linearity in stress-strain behaviour of overconsolidated soil. In *Proceedings of the 7th international conference on computer methods and advances in geomechanics, Cairns, Queensland, Australia* (eds G. Beer, J. R. Booker and J. P. Carter), vol. 1, pp. 555–568. Rotterdam, the Netherlands: Balkema.
- Burland, J. B. (1990). On the compressibility and shear strength of natural clays. 30th Rankine lecture. *Géotechnique* **40**, No. 3, 329–378, <http://dx.doi.org/10.1680/geot.1990.40.3.329>.
- Burland, J. B., Rampello, S., Georgiannou, V. N. & Calabresi, G. (1996). A laboratory study of the strength of four stiff clays. *Géotechnique* **46**, No. 3, 491–514, <http://dx.doi.org/10.1680/geot.1996.46.3.491>.
- Callerio, A., Janicki, K., Milani, D., Priano, S. & Signori, M. (2013). Cross-hole tests at Zelazny Most tailings pond, Poland – Highlights and statistical interpretation of results. *Proceedings of the 19th European meeting of environmental and engineering geophysics, Bochum, Germany*. Houten, the Netherlands: European Association of Geoscientists and Engineers.
- Chandler, R. J. (1977). Back analysis techniques for slope stabilization works: a case record. *Géotechnique* **27**, No. 4, 479–495, <http://dx.doi.org/10.1680/geot.1977.27.4.479>.
- Chandler, R. J. (2000). Clay sediments in depositional basins; 3rd Glossop lecture; the geotechnical cycle. *Q. J. Engng Geol. Hydrogeol.* **33**, No. 1, 7–39.
- Chandler, R. J. (2010). Stiff sedimentary clays: geological origins and engineering properties. *Géotechnique* **60**, No. 12, 891–902, <http://dx.doi.org/10.1680/geot.07.KP001>.
- Chandler, R. J., Jamiolkowski, M., Faiella, D., Ridley, A. M. & Rocchi, G. (2011). Suction measurements on undisturbed samples of heavily overconsolidated clays. *Proceedings of the XXIV convegno nazionale di geotecnica, Napoli*. Bologna, Italy: Patron Editore.
- Cotecchia, F. & Chandler, R. J. (1997). The influence of structure on the pre-failure behaviour of a natural clay. *Géotechnique* **47**, No. 3, 523–544, <http://dx.doi.org/10.1680/geot.1997.47.3.523>.
- DiBiagio, E. & Strout, J. M. (2013). *Expert advisory services – Zelazny Most tailings dam instrumentation*, NGI Report no. 201220750-4, presentation of piezometers data by consultant at IBE meeting. Oslo, Norway: Norwegian Geotechnical Institute.
- Dyvik, R. (1998). *Triaxial tests of undisturbed and reconstituted specimens of tailings*. Oslo, Norway: Norwegian Geotechnical Institute.
- Dyvik, R. & Høeg, K. (1999). Comparison of tests on undisturbed and reconstituted silt and silty sand. In *Proceedings of workshop on physics and mechanics of soil liquefaction* (eds P. V. Lade and J. A. Yamamuro), pp. 159–167. Baltimore, MD, USA: Balkema.
- Feng, T. W. (1991). *Compressibility and permeability of natural soft clays and surcharging to reduce settlements*. PhD thesis, University of Illinois at Urbana–Champaign, Urbana, IL, USA.
- Georgiannou, V. N. & Burland, J. B. (2001). A laboratory study of post rupture strength. *Géotechnique* **51**, No. 8, 665–676, <http://dx.doi.org/10.1680/geot.2001.51.8.665>.
- Gibo, S., Egashira, K., Ohtsubo, M. & Nakamura, S. (2002). Strength recovery from state in reactivated landslides. *Géotechnique* **52**, No. 9, 683–686, <http://dx.doi.org/10.1680/geot.2002.52.9.683>.
- Høeg, K., Dyvik, R. & Sandbækken, G. (2000). Strength of undisturbed versus reconstituted silt and silty sand specimens. *J. Geotech. Geoenviron. Engng, ASCE* **126**, No. 7, 606–617.
- Hutchinson, J. N. (1995). The significance of tectonically produced pre-existing shears. *Proceedings of the XI European conference on soil mechanics and foundation engineering, Copenhagen, Denmark*, vol. 4, pp. 59–67. Lyngby, Denmark: Danish Geotechnical Society.
- Idriss, I. & Boulanger, R. W. (2008). *Soil liquefaction during earthquakes*, monograph MNO-12. Oakland, CA, USA: Earthquake Engineering Research Institute.
- Ishihara, K. (1993). Liquefaction and flow failure during earthquake. 33rd Rankine lecture. *Géotechnique* **43**, No. 3, 351–415, <http://dx.doi.org/10.1680/geot.1993.43.3.351>.
- Ishihara, K., Huang, Y., Tsuchiya, H., & Abousleiman, Y. (1998). Liquefaction resistance of nearly saturated sand as correlated with longitudinal wave velocity. In *Proceeding of the 1st conference on poromechanics: A tribute to Maurice A. Biot, Louvain-la-Neuve, Belgium* (eds J. F. Thimus, O. Coussy and E. Detournay), pp. 583–586. Leiden, the Netherlands: Balkema/CRC Press.
- Ishihara, K., Tsukamoto, Y. & Kamada, K. (2004). Undrained behaviour of near-saturated sand in cyclic and monotonic loading. In *Proceedings of international conference on cyclic behaviour of soils and liquefaction phenomena, Bochum, Germany* (ed. T. Triantafyllidis), pp. 27–40. London, UK: Taylor & Francis.
- Jamiolkowski, M. (2012). Role of geophysical testing in geotechnical site characterization; 3rd De Mello lecture, Portuguese-Brazilian geotechnical congress. *Soils and Rocks* **35**, No. 2, 117–140.
- Jamiolkowski, M., Carrier, W. D., Chandler, R. J., Høeg, K., Swierczynski, W., & Wolski, W. (2010). The geotechnical problems of the second world largest copper tailings pond at Zelazny Most, Poland. Za-Chieh Moh distinguished lecture keynote speech. In *Proceedings of the 17th SEAGC South East Asian Geotechnical Conference, Taipei, Taiwan* (eds J. C. C. Li and M. L. Lin), vol. 2, pp. 12–27. Taipei, Taiwan: Taiwan Geotechnical Society.
- Kovacevic, N., High, D. W. & Potts, D. M. (2004). Temporary slope stability in London clay – back analyses of two case histories. In *Proceedings of the Skempton conference on advances in geotechnical engineering, London, UK* (eds R. J. Jardine, D. M. Potts and K. G. Higgins), vol. 3, pp. 1–14. London, UK: Thomas Telford.
- Kovacevic, N., Potts, D. M. & Carter, I. C. (2013). Finite-element analysis of the failure and reconstruction of the main dam embankment at Abberton Reservoir, Essex, UK. *Géotechnique* **63**, No. 9, 753–767, <http://dx.doi.org/10.1680/geot.12.P066>.
- Lipinski, M. J. (2000). *Undrained response of cohesionless soils to monotonic loading*. PhD thesis, Technical University of Gdansk, Poland.
- Lipinski, M. J. (2012). *Laboratory tests on undisturbed samples of tailings from Zelazny Most tailings pond*, Report 144/2645/10. Warsaw, Poland: Geoteko Geotechnical Consultants Ltd.
- Liu, N. & Mitchell, J. K. (2006). Influence of non-plastic fines on shear wave velocity-based assessment of liquefaction. *J. Geotech. Geoenviron. Engng, ASCE* **132**, No. 8, 1091–1097.
- Lupini, J. F., Skinner, A. E. & Vaughan, P. K. (1981). The drained residual strength of cohesive soils. *Géotechnique* **31**, No. 2, 181–213, <http://dx.doi.org/10.1680/geot.1981.31.2.181>.

- Marchetti, S., Monaco, P., Totani, G. & Marchetti, D. (2008). In situ tests by seismic dilatometer (SDMT). In *From research to practice in geotechnical engineering, honours Dr John H. Schmertmann* (eds J. E. Laier, D. K. Crapps and M. H. Hussein), Geotechnical Special Publication GSP 180, pp. 291–311. Reston, VA, USA: ASCE.
- Mikkelsen, P. E. & Green, G. E. (2003). Piezometers in fully grouted boreholes. In *Proceedings of the 6th international symposium on field measurements in geomechanics, Oslo, Norway* (ed. F. Myrvoll), pp. 545–554. Lisse, the Netherlands: Balkema.
- Morgenstern, N. R. & Tchalenko, J. S. (1967). Micro-structural analysis on shear zones from slips in natural clays. Shear strength properties of natural soils and rocks. *Proceedings of the 4th European conference on soil mechanics and foundation engineering* (eds N. Janbu and Norwegian Geotechnical Institute), Oslo, Norway, pp. 147–152. Oslo, Norway: Aas & Wahls Boktrykkeri.
- Nakazawa, H., Ishihara, K., Tsukamoto, Y. & Kamata, T. (2004). Case studies on evaluation of liquefaction resistance of imperfectly saturated soil deposits. In *Proceedings of the international conference on cyclic behaviour of soils and liquefaction phenomena*, Bochum, Germany (ed. T. Triantafyllidis), pp. 295–304. London, UK: Taylor & Francis.
- NGI (Norwegian Geotechnical Institute) (2010). *Finite element analysis of Zelazny Most tailings dam – static stability and deformation of section XVIIE*, Report no. 20091019-0012-R. Oslo, Norway: Norwegian Geotechnical Institute.
- NGI (2011). *FEA of Zelazny Most tailings dam – stability and deformation of section XVIIE: Effects of creep, strain softening and dynamic loading*, Report no. 20100553-00-1-R. Oslo, Norway: Norwegian Geotechnical Institute.
- NGI (2013a). *FEA stability of Zelazny Most tailings dam of section XVIIE: Analyses with creep in the tertiary clay and strain softening in the shear zones*, Report no. 20120177-02-R. Oslo, Norway: Norwegian Geotechnical Institute.
- NGI (2013b). *FEA of Zelazny Most tailings dam – situation with deep vertical shafts – effects of vertical shafts on stability and displacements*, Report no. 20120742-01-R. Oslo, Norway: Norwegian Geotechnical Institute.
- Olson, S. M. (2001). *Liquefaction analysis of level and sloping ground using field case histories and penetration resistance*. PhD thesis, University of Illinois at Urbana–Champaign, Urbana, IL, USA.
- Peck, R. B. (1969). Advantages and limitations of the observational method in applied soil mechanics. 9th Rankine lecture. *Géotechnique* **19**, No. 2, 171–187, <http://dx.doi.org/10.1680/geot.1969.19.2.171>.
- Peck, R. B. (1980). Where has all the judgment gone? The Fifth Laurits Bjerrum memorial lecture. *Can. Geotech. J.* **17**, No. 4, 584–590.
- Potts, D. M., Dounias, G. T. & Vaughan, P. R. (1990). Finite element analysis of progressive failure of Carsington embankment. *Géotechnique* **40**, No. 1, 79–101, <http://dx.doi.org/10.1680/geot.1990.40.1.79>.
- Potts, D. M., Kovacevic, N. & Vaughan, P. R. (1997). Delayed collapse of cut slopes in stiff clay. *Géotechnique* **47**, No. 5, 953–982, <http://dx.doi.org/10.1680/geot.1997.47.5.953>.
- Ridley, A. M. & Burland, J. B. (1993). A new instrument for the measurement of soil moisture suction. *Géotechnique* **43**, No. 2, 321–324, <http://dx.doi.org/10.1680/geot.1993.43.2.321>.
- Ridley, A. M. & Burland, J. B. (1995). Measurement of suction in materials which swell. *Appl. Mech. Rev.* **48**, No. 10, 727–732.
- Robertson, P. K., Woeller, D. J. & Finn, W. D. L. (1992). Seismic cone penetration test for evaluating liquefaction potential under cyclic loading. *Can. Geotech. J.* **29**, No. 4, 686–695.
- Robertson, P. K., Sasitharan, S., Cuning, J. C. & Sego, D. C. (1995). Shear-wave velocity to evaluate in-situ state of Ottawa sand. *J. Geotech. Geoenviron. Engng, ASCE* **121**, No. 3, 262–273.
- Rocchi, G., Vaciago, G., Callerio, A., Fontana, M. & Previtali, R. (2012). Geotechnical aspects of landslide triggering. In *Safeland deliverable 1.1 rev. no. 2: landslide triggering mechanisms in Europe – overview and state of the art; 7th framework programme, cooperation theme 6 environment (including climate change), sub activity 6.1.3 natural hazards*. See http://www.safeland-fp7.eu/results/Documents/D1.1_revised.pdf (accessed 17/09/2014).
- Rocchi, G., Vaciago, G., Callerio, A. & Fontana, M. (2013). Description of soils based on geomechanical criteria for improved landslide classification. *Landslides*, <http://dx.doi.org/10.1007/s10346-013-0439-8>.
- Rocchi, G. & Da Prat, M. (2014). *Zelazny Most copper tailings dam: Stability and deformation finite element analysis*, Internal Report. Milan, Italy: Studio Geotecnico Italiano.
- Skempton, A. W. (1954). The pore-pressure coefficients A and B. *Géotechnique* **4**, No. 4, 143–147, <http://dx.doi.org/10.1680/geot.1954.4.4.143>.
- Skempton, A. W. (1985). Residual strength of clays in landslides, flooded strata and the laboratory. *Géotechnique* **35**, No. 1, 3–18, <http://dx.doi.org/10.1680/geot.1985.35.1.3>.
- Skempton, A. W. & Hutchinson, J. N. (1969). Stability of natural slopes and embankment foundations. In *State of the art, Proceedings of the VII international conference on soil mechanics and foundation engineering*, Mexico City, vol. 4, pp. 291–340. Mexico City, Mexico: Sociedad Mexicana de Mecanica de Suelos.
- Skempton, A. W. & Petley, D. J. (1967). The strength along structural discontinuities in stiff clays. In *Shear strength properties of natural soils and rocks, Proceedings of IV European conference on soil mechanics and foundation engineering* (eds N. Janbu and Norwegian Geotechnical Institute), Oslo, Norway, vol. 2, pp. 29–46. Oslo, Norway: Aas & Wahls Boktrykkeri.
- Stallebrass, S. E. & Taylor, R. N. (1997). The development and evaluation of a constitutive model for the prediction of ground movements in overconsolidated clay. *Géotechnique* **47**, No. 2, 235–253, <http://dx.doi.org/10.1680/geot.1997.47.2.235>.
- Takahashi, H., Kitazume, M., Ishibashi, S. & Yamawaki, S. (2006). Evaluating the saturation of model ground by P-wave velocity and modelling of models for a liquefaction study. *Int. J. Phys. Modelling Geotech.* **6**, No. 1, 13–25.
- Tavenas, F., Jean, P., Leblond, P. & Leroueil, S. (1983). The permeability of natural soft clays. Part II: permeability characteristics. *Can. Geotech. J.* **20**, No. 4, 645–660.
- Taylor, D. W. (1948). *Fundamentals of soil mechanics*. New York, NY, USA: Wiley.
- Toyota, H., Nakamura, K., Sugimoto, M. & Sakai, N. (2009). Ring shear tests to evaluate strength parameters in various remoulded soils. *Géotechnique* **59**, No. 8, 649–659, <http://dx.doi.org/10.1680/geot.8.029.3671>.
- Tsukamoto, Y., Ishihara, K., Nakazawa, H., Kamada, K. & Huang, Y. (2002). Resistance of partly saturated sand to liquefaction with reference to longitudinal and shear wave velocities. *Soils Found.* **42**, No. 6, 93–104.
- Valle-Molina, C. (2006). *Measurements of V_p and V_s in dry, unsaturated and saturated sand specimens with piezoelectric transducers*. PhD thesis, University of Texas at Austin, Austin, TX, USA.
- Vaughan, P. R. (1969). Note on sealing piezometers in boreholes. *Géotechnique* **19**, No. 3, 405–413, <http://dx.doi.org/10.1680/geot.1969.19.3.405>.
- Vermeer, P. A. & De Borst, R. (1984). Non associated plasticity for soils. *Concrete and Rock (Heron)* **29**, No. 3, 3–64.
- Wedage, A. M. P., Morgenstern, N. R. & Chan, D. H. (1998). Simulation of time-dependent movements in Syncrude tailings dyke foundation. *Can. Geotech. J.* **35**, No. 2, 284–298.